

# Controlling Chemical Reactivity with Optimally Oriented Electric Fields: A Generalisation of the Newton Trajectory Method

Josep Maria Bofill,<sup>\*,†,‡</sup> Wolfgang Quapp,<sup>\*,¶</sup> Guillermo Albareda,<sup>\*,‡,§</sup> Ibério de P.R.  
Moreira,<sup>\*,‡,||</sup> and Jordi Ribas-Ariño<sup>\*,‡,||</sup>

<sup>†</sup>*Departament de Química Inorgànica i Orgànica, Secció de Química Orgànica*

<sup>‡</sup>*Institut de Química Teòrica i Computacional, (IQTCUB), Universitat de Barcelona,  
Martí i Franquès 1, 08028 Barcelona, Spain*

<sup>¶</sup>*Mathematisches Institut, Universität Leipzig, PF 100920, D-04009 Leipzig, Germany*

<sup>§</sup>*Max Planck Institute for the Structure and Dynamics of Matter and Center for Free  
Electron Laser Science, Luruper Chaussee 149, 22761 Hamburg, Germany*

<sup>||</sup>*Departament de Ciència de Materials i Química Física, Secció de Química Física,  
Universitat de Barcelona, Martí i Franquès 1, 08028 Barcelona, Spain*

E-mail: jmbofill@ub.edu; quapp@math.uni-leipzig.de; guillermo.albareda@mpsd.mpg.de;  
i.moreira@ub.edu; j.ribas@ub.edu

## Abstract

The use of oriented external electric fields (OEEF) as a tool to accelerate chemical reactions has recently attracted a lot of interest. A new model to calculate the *optimal OEEF* of the least intensity to induce a barrierless chemical reaction path is

presented. A suitable ansatz is provided by defining an effective potential energy surface (PES) which considers the unperturbed or original PES of the molecular reactive system and the action of a constant OEEF on the overall dipole moment of system. Based on a generalization of the Newton Trajectories (NT) method it is demonstrated that the *optimal OEEF* can be determined upon locating a special point of the potential energy surface (PES), the so-called *optimal bond-breaking-point (optimal BBP)*, for which two different algorithms are proposed. At this point, the gradient of the original or unperturbed PES is an eigenvector of zero eigenvalue of the Hessian matrix of the effective PES. A thorough discussion of the geometrical aspects of the *optimal BBP* and the *optimal OEEF* is provided using a 2-dimensional model, and numerical calculations of the *optimal OEEF* for a  $S_N2$  reaction and the 1,3-dipolar retrocycloaddition of isoxazole to fulminic acid plus acetylene reaction serve as a proof-of-concept. The knowledge of the orientation of *optimal OEEF* provides a practical way to reduce the effective barrier of a given chemical process.

## Introduction.

The interaction of external electric fields with atoms, molecules and materials results in multiple phenomena<sup>1-5</sup> such as the Stark effect,<sup>6-8</sup> orientation of liquid-crystalline materials,<sup>9</sup> spin-polarized electrical currents,<sup>10</sup> control of supramolecular networks adsorbed on surfaces,<sup>11</sup> controlled rotation, isomerization, tautomerization or conformational rearrangements of molecules that can be harnessed in molecular switches,<sup>12-17</sup> spin transitions,<sup>18</sup> electrostatic catalysis,<sup>2-5,19</sup> enhancement or suppression of the signals in spectroscopy.<sup>20</sup> The great potential of oriented external electric fields (OEEF) as a tool for catalyzing reactions, as well as for controlling their selectivity, has been long advocated by several pioneering computational studies.<sup>21-26</sup> In a recent landmark single-molecule experiment by Aragonès et al.,<sup>27</sup> it was demonstrated that OEEFs created by a bias voltage between an electrode and an scanning tunnelling microscopy tip can catalyze a Diels-Alder reaction, in line with

the predictions previously made by Shaik and coworkers in a computational work.<sup>25</sup> Subsequent single-molecule experiments have also shown that OEEFs can promote homolysis of alkoxyamines<sup>28</sup> and aromatization reactions.<sup>29</sup> Other experimental techniques designed to exploit electric fields in chemical processes with a higher potential for scalability<sup>19</sup> include the use of interfacial electric fields in electrochemical cells<sup>30–32</sup> and the use of a charged functional group attached to one of the species involved in the reaction.<sup>33,34</sup>

The effects of external electric fields (EEFs) on reactivity have been intensively investigated by computational means in recent years. Calculations based on a rigorous inclusion of the effect of a given electric field on the electrons and nuclei have predicted that EEFs can catalyze many types of reactions (eg., Diels–Alder reactions,<sup>25,35,36</sup> other types of cycloaddition reactions,<sup>37</sup> the Menshutkin reaction,<sup>38</sup> ring-opening reactions,<sup>39</sup> electrophilic aromatic substitution reactions,<sup>40</sup> oxidative addition reactions between palladium catalysts and alkyl/aryl electrophiles,<sup>41</sup> the Kemp elimination reaction,<sup>42</sup> thermal and photo isomerization of azobenzene,<sup>43</sup> degradation of bromobenzene<sup>44</sup>), improve the efficiency of heterogeneous catalysts,<sup>45,46</sup> control the selectivity of reactions,<sup>23–25,35,47</sup> cause drastic changes in reaction mechanisms<sup>25,40</sup> and induce conformational rearrangements.<sup>48</sup> All these effects can be understood on the basis of the ionicity induced by EEFs on bonds and transition states, which, in turn, can be rationalized using a valence bond perspective.<sup>2–5</sup> The effect of OEEFs on reactivity can also be rationalized by using quantitative activation strain and Kohn–Sham molecular orbital theory, as recently shown by Bickelhaupt and coworkers.<sup>35</sup> The computational work performed so far has also shown that the orientation of the EEF is essential for a proper control of the rate and outcome of a given reaction. Despite the acknowledged importance of the orientation of the EEF and the in-depth understanding of the impact of EEFs on reactivity achieved so far, there is a crucial question that, to the best of our knowledge, has not been yet addressed. Specifically, what is the *optimally oriented EEF* (*optimal OEEF*) that yields a barrierless chemical path with the least intensity? A

theoretical model to establish such an *optimal OEEF* for a given chemical process is missing.

In this article, we propose two algorithms to find *optimal OEEFs*. In contrast to previous computational works in which the effect of OEEFs is considered only on transition states (TSs) and reactant configurations, our algorithm considers a continuous curve that, by construction, joins the reactant and product configurations through a special topological point (referred to as *optimal bond breaking point*, (*optimal BBP*)) from which the information regarding the *optimal OEEF* will be obtained. Our algorithm, which is rooted in previous theoretical works on Mechanochemistry and the concept of Newton trajectory (NT), uses an effective continuous curve built from the unperturbed potential energy surface (PES) of the molecular reactive system and the action of a constant external electric field on the overall dipole moment of the system. The algorithm herein presented is not only relevant for optimally harnessing OEEFs in promoting reactions but it is also relevant in the whole field of catalysis. In fact, electric fields in the active sites of enzymes, which are the result of the nearby distribution of the residues of the enzyme and also from the surrounding solvent, are being increasingly recognized as a major driving force in the catalytic activity of enzymes.<sup>49-54</sup> It should be stressed here that optimization of catalysts (including enzymes, heterogeneous catalysts and supramolecular structures) on the basis of the electric field acting on the substrate holds great promise when it comes to designing efficient chemical processes.<sup>55-57</sup>

The structure of the present work is as follows: in the next Section ‘A Brief Summary on the Newton Trajectory Model applied to Mechanochemistry. The existence of Bond Breaking Points’, we will briefly summarize a set of basic concepts of NTs applied to Mechanochemistry to set the stage for the presentation of the algorithm devised to find *optimal OEEFs*. In Section ‘Optimally Oriented External Electric Field. An Extension of Newton Trajectory Model’, we will provide the basic ansatz in which our algorithm is based to include the effect

of an OEEF in the unperturbed PES, as well as its mathematical structure. In Section ‘Two Algorithms to Find the Optimally Oriented External Electric Field’, we develop the method for the calculation of an optimal field,  $\mathbf{e} = (e_x, e_y, e_z)^T$ , based on the basic ansatz and a series of iterated steps. Here it is shown that the determination of the *optimal BBP* of the PES of a given molecule<sup>58,59</sup> and the COGEF method<sup>60</sup> for the determination of the moved stationary points play an essential role in the algorithm. A thorough analysis of the main geometrical aspects of the *optimal BBP* and the *optimal OEEF* as compared with well established concepts in Mechanochemistry is presented in Section ‘A thorough discussion of the main geometrical aspects of the optimal BBP and the optimal OEEF’ for a 2-dimensional simplified PES. In Section ‘Application of the Algorithm to Realistic Chemical Examples’, we report two examples, namely, the ‘An  $S_N2$  reaction of the amine attack on chloromethane’ and the ‘1,3-Dipolar Retrocycloaddition of of Isoxazole to Fulminic Acid plus Acetylene’. These two examples provide a proof-of-concept application of the method to two chemical reactions. Finally, the remarks and conclusions of this work are provided in Section ‘Conclusions’.

# 1 A Brief Summary of the Newton Trajectory Model applied to Mechanochemistry. The existence of Bond Breaking Points.

In this Section we will introduce the basic concepts of the Newton Trajectory model applied to Mechanochemistry.<sup>61–67</sup> These concepts will serve later as the basis of the model to establish *optimal OEEFs*. We start by considering a constant mechanical external force acting on a molecular system. It is well known that the applied force modifies or transforms the PES of the system according to the following expression:<sup>68,69</sup>

$$V_{\mathbf{f}}(\mathbf{x}) = V(\mathbf{x}) - \mathbf{f}^T \cdot \mathbf{x} = V(\mathbf{x}) - F \mathbf{f}_n^T \cdot \mathbf{x} = V(\mathbf{x}) - F (f_1, \dots, f_N)_n \cdot \mathbf{x}, \quad (1)$$

where  $V(\mathbf{x})$  is the original or unperturbed PES and  $\mathbf{x}^T = (x_1, y_1, z_1, \dots, x_M, y_M, z_M)$  is the vector of all  $M$  atoms' Cartesian coordinates. We define  $N = 3M$  as the total number of Cartesian coordinates. The fixed force vector  $\mathbf{f} = F \mathbf{f}_n$  points along the normalized or unit direction,  $\mathbf{f}_n^T = (f_1, \dots, f_N)_n$ , and has a modulus  $F$ . The superscript  $T$  denotes the transpose.

The external force will result in a distortion of the structures of the original minimums and saddle points (SPs). The new stationary points on the effective potential satisfy the condition  $\nabla_{\mathbf{x}} V_{\mathbf{f}}(\mathbf{x}) = \mathbf{0}$ , which implies:

$$\nabla_{\mathbf{x}} V_{\mathbf{f}}(\mathbf{x}) = \mathbf{g}(\mathbf{x}) - F \mathbf{f}_n = \mathbf{0} . \quad (2)$$

This means that in the new set of stationary points of  $V_{\mathbf{f}}(\mathbf{x})$ , the gradient of the original PES,  $\mathbf{g}(\mathbf{x})$ , has to be equal to the external force  $\mathbf{f}$ . Given an external force with a fixed direction  $\mathbf{f}_n$ , the set of stationary points for each different value of  $F$  characterizes the so-called Newton trajectory<sup>61,62</sup> (NT). Consequently, the NT describes a curve of force-displaced stationary points (FDSPs) of the tilted PES under a different load,  $F$ .<sup>61-67</sup> For a properly chosen force direction, the energy of minimums is increased, and the energy of the SP is lowered.<sup>70</sup> This results in a force-induced lowering of the energy barriers. Every NT describes a connection between different stationary points of an index difference of one.<sup>71</sup> Following numerically an NT is a method to search a next SP if a minimum is given, or vice versa. It can be shown that the tangent equation of the NT curve is given by<sup>62,64</sup>

$$(\mathbf{U} - \mathbf{f}_n \mathbf{f}_n^T) \mathbf{H}(\mathbf{x}) \frac{d\mathbf{x}}{dt} = \mathbf{0} . \quad (3)$$

Where  $t$  is the parameter that characterizes the curve,  $\mathbf{x}(t)$  and  $\mathbf{U}$  is the unit matrix. Note that the Hessian,  $\mathbf{H}(\mathbf{x})$ , is the same for all effective PES and different values of  $F$  because  $\mathbf{f}_n$  is constant. Eq. (3) is an equation for the tangent of the FDSPs curve.

If one starts at a minimum with  $F = 0$  and increases the magnitude of the force  $F$  in order to move along the FDSPs path, we get a sub-arc of this path leading uphill from the minimum, and we get another analogous sub-arc leading downhill from the saddle point of index 1 ( $SP_1$ ). Usually, the two arcs will meet at the point where the gradient norm achieves its maximal value. This meeting point is named barrier breakdown point (BBP). At such points holds that  $Det[\mathbf{H}(\mathbf{x})] = 0$ .<sup>66,72</sup> Furthermore, at the BBPs the norm of the gradient of the PES along the NT reaches a turning point, and the effective surface  $V_{\mathbf{f}}(\mathbf{x})$  presents a shoulder on the FDSPs path. The shoulder is the result of the coalescence of minimum and  $SP_1$ . From a mathematical point of view the BBP concept is strongly related with Catastrophe Theory.<sup>58,59,72-75</sup> For different NTs we have different BBPs, all of them defining a manifold. Within this manifold there is an *optimal BBP*,<sup>66,76</sup> (compare Figs. 2-4 and 6 of Ref. 66). This *optimal BBP* defines the lowest force in magnitude and the corresponding pulling direction that should be applied in order to mechanically promote a given chemical transformation by making it barrierless. The *optimal BBP* satisfies the equation<sup>66</sup>

$$\mathbf{H}(\mathbf{x})\mathbf{g}(\mathbf{x}) = \mathbf{0} \tag{4}$$

where  $\mathbf{g}(\mathbf{x}) \neq \mathbf{0}$ . Note that here the *optimal BBP* is a property of the Hessian of the original PES. The force,  $\mathbf{f}$ , does not appear in its determination. The reason is the linearity of the ansatz given in Eq. (1) with respect to  $\mathbf{f}$ . Thus, the force does not appear in the Hessian when it is differentiated in  $\mathbf{x}$ . At the *optimal BBP* (hereafter also labeled as oBBP) the gradient is an eigenvector of the Hessian matrix with null eigenvalue. The *optimal BBP*, labeled as  $\mathbf{x}_{oBBP}$ , coincides with a point of the gradient extremal (GE)<sup>77-79</sup> exactly at the intersection point with the  $Det[\mathbf{H}(\mathbf{x})] = 0$ -manifold.<sup>66,76</sup> Eq. (4) is an eigenvalue equation where the eigenvalue is zero of the eigenvector  $\mathbf{g}(\mathbf{x})$  at  $\mathbf{x} = \mathbf{x}_{oBBP}$ . The location of oBBPs is extremely important in the context of Mechanochemistry<sup>58,59</sup> because these points reveal which is the most efficient way to trigger a reaction by means of a mechanical force. In other words, the

gradient vector satisfying Eq. (4), namely,  $\mathbf{g}(\mathbf{x}_{oBBP})$  is the vector which characterizes the optimal force,  $\mathbf{f}$ , since from Eq. (2) we can write,  $\mathbf{g}(\mathbf{x}_{oBBP}) = \mathbf{f}_n^* F_c$ . Below we demonstrate that an analogous expression still holds for electrically triggered transformations.

## 2 Optimally Oriented External Electric Field. An Extension of the Newton Trajectory Model.

Like in Mechanochemistry, the OEEF modifies the original PES. We will assume that the perturbed PES by the external electric field,  $\mathbf{e} = E \mathbf{e}_n$ , with modulus  $E$  and direction  $\mathbf{e}_n$ , is given by the following ansatz:

$$V_e(\mathbf{x}) = V(\mathbf{x}) - \mathbf{e}^T \cdot \mathbf{d}(\mathbf{x}) = V(\mathbf{x}) - E \mathbf{e}_n^T \cdot \mathbf{d}(\mathbf{x}) = V(\mathbf{x}) - E (e_x, e_y, e_z)_n \cdot \mathbf{d}(\mathbf{x}) , \quad (5)$$

where,  $\mathbf{d}(\mathbf{x})$  is the dipole moment vector. The multiplication point between the 3-dimensional normalized field direction vector  $\mathbf{e}_n^T = (e_x, e_y, e_z)_n$  and the dipole vector  $\mathbf{d}(\mathbf{x})$  denotes a scalar product. The dipole vector is a three component vector where each component depends (usually in a non-linear manner) on the  $\mathbf{x}$ -vector,  $\mathbf{d}^T(\mathbf{x}) = (d_x(\mathbf{x}), d_y(\mathbf{x}), d_z(\mathbf{x}))$ .

It should be emphasized that Eq. (5) is qualitatively different from Eq. (1) due to the emergence of the nonlinear vector function  $\mathbf{d}(\mathbf{x})$ . In an analogous way to Mechanochemistry the OEEF will distort the stationary points of the original PES. These distortions will be controlled by the gradient of  $V_e(\mathbf{x})$ , which will adopt a different structure to the gradient model applied in Mechanochemistry (c.f. Eq. (2)) due to the  $E \mathbf{e}_n^T \cdot \mathbf{d}(\mathbf{x})$  summand. The stationary condition  $\nabla_{\mathbf{x}} V_e(\mathbf{x}) = \mathbf{0}$  now is:

$$\nabla_{\mathbf{x}} V_e(\mathbf{x}) = \mathbf{g}(\mathbf{x}) - [\nabla_{\mathbf{x}} \mathbf{d}^T(\mathbf{x})] \cdot E \mathbf{e}_n = \mathbf{0} . \quad (6)$$

Where  $[\nabla_{\mathbf{x}} \mathbf{d}^T(\mathbf{x})]$  is a matrix of dimension  $(N \times 3)$ . Let us now consider a FDSPs curve

(i.e., a set of points obtained for several values of  $E$  assuming a fixed direction of the OEEF) built from Eq. (6). The next two questions emerge: will the direction of the gradient be parallel to  $\mathbf{e}$  at each point of the curve? And if not, is  $\mathbf{e}$  parallel to some kind of vector? The answer to the first question is no. This is due to the existence of the  $[\nabla_{\mathbf{x}} \mathbf{d}^T(\mathbf{x})]$  matrix, which is different from the unit matrix. Note that this in stark contrast with the previously described Mechanochemistry model, for which the gradient of the original PES is parallel to the external force with a given fixed direction at all points of the FDSPs curve. To answer the second question we have to prove that there is a vector parallel to  $\mathbf{e}$  at each point of the FDSPs curve. For this purpose we multiply Eq. (6) from the left by  $[\nabla_{\mathbf{x}} \mathbf{d}^T(\mathbf{x})]^T$ . After rearranging the resulting expression, we obtain the following equation, which is analogous to Eq. (6):

$$\mathbf{e} = E \mathbf{e}_n = \mathbf{P}(\mathbf{x}) \cdot \mathbf{g}(\mathbf{x}) , \quad (7)$$

where

$$\mathbf{P}(\mathbf{x}) = \left\{ [\nabla_{\mathbf{x}} \mathbf{d}^T(\mathbf{x})]^T [\nabla_{\mathbf{x}} \mathbf{d}^T(\mathbf{x})] \right\}^{-1} [\nabla_{\mathbf{x}} \mathbf{d}^T(\mathbf{x})]^T . \quad (8)$$

has dimension of  $(3 \times N)$  and it exists if and only if  $Det\left\{ [\nabla_{\mathbf{x}} \mathbf{d}^T(\mathbf{x})]^T [\nabla_{\mathbf{x}} \mathbf{d}^T(\mathbf{x})] \right\} \neq 0$ . The  $\mathbf{P}(\mathbf{x})$  matrix will denote a pseudo-inverse matrix.<sup>80,81</sup> Eq. (7) is formally equivalent to Eq. (2) used in Mechanochemistry if one does the following two equivalences:  $F \mathbf{f}_n \leftrightarrow E \mathbf{e}_n$  and  $\mathbf{g}(\mathbf{x}) \leftrightarrow \mathbf{P}(\mathbf{x})\mathbf{g}(\mathbf{x})$ . Thus, in the context of OEEFs, the vector parallel to the constant direction of electric field in all points of the FDSPs curve is not the gradient alone (like in the Mechanochemistry model), but the  $\mathbf{P}(\mathbf{x})\mathbf{g}(\mathbf{x})$  transformed gradient. The model herein presented can thus be considered as an extension of the NT model.

After having found the stationarity condition of FDSPs for OEEF, we will now focus on the derivation of the tangent expression that is equivalent to that found in the previous Mechanochemistry model (c.f. Eq. (3)). This tangent is important for the integration of the FDSPs curve under the action of an OEEF. The task is to find the curve that at each point

satisfies Eq. (6) with a fixed orientation of the external electric field. For this purpose, we first define  $\mathbf{w}(\mathbf{x}, \mathbf{e})$  as the vectorial function satisfying the condition  $\nabla_{\mathbf{x}} V_{\mathbf{e}}(\mathbf{x}) = \mathbf{0}$ . Second, we evaluate the directional derivative of  $\mathbf{w}(\mathbf{x}, \mathbf{e})$  with respect to  $\mathbf{x}$  and  $\mathbf{e}$  at the point  $(\mathbf{x}, \mathbf{e}) = (\mathbf{x}(t), \mathbf{e}_n E(t))$  where a step length parameter,  $t$ , is in  $t_0 \leq t \leq t_f$ . This is the external oriented electric field condition:

$$\begin{aligned} \left. \frac{d\mathbf{w}^T(\mathbf{x}, \mathbf{e})}{dt} \right|_{\mathbf{x}=\mathbf{x}(t), \mathbf{e}=\mathbf{e}_n E(t)} &= \begin{pmatrix} d\mathbf{x}^T/dt, & d\mathbf{e}^T/dt \end{pmatrix} \begin{pmatrix} \nabla_{\mathbf{x}} \\ \nabla_{\mathbf{e}} \end{pmatrix} \mathbf{w}^T(\mathbf{x}, \mathbf{e}) \Big|_{\mathbf{x}=\mathbf{x}(t), \mathbf{e}=\mathbf{e}_n E(t)} = \\ & \begin{pmatrix} d\mathbf{x}^T/dt, & d\mathbf{e}^T/dt \end{pmatrix} \begin{pmatrix} \mathbf{H}(\mathbf{x}) - \langle \mathbf{N}(\mathbf{x}) \mathbf{e} \rangle \\ -[\nabla_{\mathbf{x}} \mathbf{d}^T(\mathbf{x})]^T \end{pmatrix} \Big|_{\mathbf{x}=\mathbf{x}(t), \mathbf{e}=\mathbf{e}_n E(t)} = \\ & (d\mathbf{x}(t)/dt)^T \{ \mathbf{H}(\mathbf{x}(t)) - \langle \mathbf{N}(\mathbf{x}(t)) \mathbf{e}_n \rangle E(t) \} - \mathbf{e}_n^T [\nabla_{\mathbf{x}} \mathbf{d}^T(\mathbf{x})]_{\mathbf{x}=\mathbf{x}(t)}^T (dE(t)/dt) = \mathbf{0}^T . \end{aligned} \quad (9)$$

We recall that  $\mathbf{e}_n$  is the normalized constant vector obtained from Eq. (7). Taking into account that  $\mathbf{H}^T(\mathbf{x}) = \mathbf{H}(\mathbf{x})$  and  $\langle \mathbf{N}(\mathbf{x}) \mathbf{e} \rangle^T = \langle \mathbf{N}(\mathbf{x}) \mathbf{e} \rangle$ , we can rewrite the last equality of Eq. (9) in a more compact form

$$\mathbf{H}_{\mathbf{e}_n}(\mathbf{x}(t), E(t)) \frac{d\mathbf{x}(t)}{dt} = \mathbf{h}_{\mathbf{e}_n}(\mathbf{x}(t)) E'(t) \quad (10)$$

where  $E'(t) = dE(t)/dt$  and

$$\mathbf{h}_{\mathbf{e}_n}(\mathbf{x}(t)) = [\nabla_{\mathbf{x}} \mathbf{d}^T(\mathbf{x})]_{\mathbf{x}=\mathbf{x}(t)} \mathbf{e}_n \quad (11)$$

and

$$\mathbf{H}_{\mathbf{e}_n}(\mathbf{x}(t), E(t)) = \{ \mathbf{H}(\mathbf{x}(t)) - \langle \mathbf{N}(\mathbf{x}(t)) \mathbf{e}_n \rangle E(t) \} \quad (12)$$

is the Hessian of the  $V_{\mathbf{e}}(\mathbf{x})$  potential that is,  $\mathbf{H}_{\mathbf{e}_n}(\mathbf{x}, E) = \nabla_{\mathbf{x}} \nabla_{\mathbf{x}}^T V_{\mathbf{e}}(\mathbf{x})$ , evaluated at  $(\mathbf{x}^T, \mathbf{e}^T) = (\mathbf{x}^T(t), \mathbf{e}_n^T E(t))$ .  $\mathbf{N}(\mathbf{x})$  is the tensor of the second derivatives of the dipole vector with respect to  $\mathbf{x}$ . The tensor is shortened by the multiplication with the  $\mathbf{e}_n$ -vector, resulting in the matrix  $\langle \mathbf{N}(\mathbf{x}(t)) \mathbf{e}_n \rangle$ . Here we can suppress the index-gymnastics notation for tensors.

Finally, if we multiply Eq. (10) from the left by the projector

$$\left[ \mathbf{U} - \frac{\mathbf{h}_{\mathbf{e}_n}(\mathbf{x}(t))\mathbf{h}_{\mathbf{e}_n}^T(\mathbf{x}(t))}{\mathbf{h}_{\mathbf{e}_n}^T(\mathbf{x}(t))\mathbf{h}_{\mathbf{e}_n}(\mathbf{x}(t))} \right], \quad (13)$$

we obtain an expression formally equivalent to Eq. (3) of the Mechanochemistry model for the FDSPs under the action of an OEEF,

$$\left[ \mathbf{U} - \frac{\mathbf{h}_{\mathbf{e}_n}(\mathbf{x}(t))\mathbf{h}_{\mathbf{e}_n}^T(\mathbf{x}(t))}{\mathbf{h}_{\mathbf{e}_n}^T(\mathbf{x}(t))\mathbf{h}_{\mathbf{e}_n}(\mathbf{x}(t))} \right] \mathbf{H}_{\mathbf{e}_n}(\mathbf{x}(t), E(t)) \frac{d\mathbf{x}(t)}{dt} = \mathbf{0}. \quad (14)$$

The last Eq. (14) differs from Eq. (3) in that i) the projector is not constant being a function of  $\mathbf{x}$  and ii) the Hessian,  $\mathbf{H}_{\mathbf{e}_n}(\mathbf{x}(t), E(t))$ , depends of the original PES Hessian and the second derivative of dipole moment with respect to  $\mathbf{x}$  contracted with the electric field,  $\mathbf{e}$ .

Now we address the problem of FDSP curve integration under a constant OEEF,  $\mathbf{e}$ . This task implies solving Eq. (10). For this purpose we first consider the predictor step. If  $\text{Det}[\mathbf{H}_{\mathbf{e}_n}(\mathbf{x}(t), E(t))] \neq 0$  then the tangent,  $d\mathbf{x}/dt$ , is

$$\frac{d\mathbf{x}(t)}{dt} = [\mathbf{H}_{\mathbf{e}_n}(\mathbf{x}(t), E(t))]^{-1} \mathbf{h}_{\mathbf{e}_n}(\mathbf{x}(t)) E'(t). \quad (15)$$

If we are in a point of the FDSP curve, then from Eq. (6) we have that

$$E = \frac{(\mathbf{g}^T(\mathbf{x})\mathbf{g}(\mathbf{x}))^{1/2}}{(\mathbf{e}_n^T[\nabla_{\mathbf{x}}\mathbf{d}^T(\mathbf{x})]^T[\nabla_{\mathbf{x}}\mathbf{d}^T(\mathbf{x})]\mathbf{e}_n)^{1/2}} = \frac{(\mathbf{g}^T(\mathbf{x})\mathbf{g}(\mathbf{x}))^{1/2}}{(\mathbf{h}_{\mathbf{e}_n}^T(\mathbf{x})\mathbf{h}_{\mathbf{e}_n}(\mathbf{x}))^{1/2}}. \quad (16)$$

Thus,  $E(t) = E$ , and  $E'(t) \approx \Delta E/\Delta t$  can be approximated for the predictor step by the distance to the former  $E$ -value. The value of  $E'(t)$  is only a scaling of the resulting predictor direction. Usually one uses a fixed step length through the tangent normalization criterium,  $(d\mathbf{x}/dt)^T(d\mathbf{x}/dt) = 1$ . The corrector step consists in moving the predicted point through a circle centered in the previous point to a new point satisfying Eq. (6).

Now we are dealing with the special points of FDSP curve. These points appear when  $Det[\mathbf{H}_{\mathbf{e}_n}(\mathbf{x}(t), E(t))] = 0$  which implies that an eigenvector of  $\mathbf{H}_{\mathbf{e}_n}(\mathbf{x}(t), E(t))$  has eigenvalue equal zero. Let us analyze Eq.(10) when the condition  $Det[\mathbf{H}_{\mathbf{e}_n}(\mathbf{x}(t), E(t))] = 0$  is satisfied at a given point of the FDSPs curve. Let us first multiply Eq.(10) from the left by  $\mathbf{H}_{\mathbf{e}_n}(\mathbf{x}(t), E(t))$ . Using Eqs.(6), (11) and that  $E(t) \neq 0$  since  $\mathbf{g}(\mathbf{x}(t)) \neq \mathbf{0}$  and  $\mathbf{e} \neq \mathbf{0}$  we have,

$$\mathbf{H}_{\mathbf{e}_n}^2(\mathbf{x}(t), E(t)) \frac{d\mathbf{x}(t)}{dt} = \mathbf{H}_{\mathbf{e}_n}(\mathbf{x}(t), E(t)) \mathbf{g}(\mathbf{x}(t)) \frac{E'(t)}{E(t)}. \quad (17)$$

As noted above, at this point, the matrix  $\mathbf{H}_{\mathbf{e}_n}(\mathbf{x}(t), E(t))$  has an eigenvector with eigenvalue equal zero. Let us assume that this eigenvector is the gradient vector,  $\mathbf{g}(\mathbf{x}(t))$ , thus the right-hand side part of Eq.(17) is zero and reduces to  $\mathbf{H}_{\mathbf{e}_n}^2(\mathbf{x}(t), E(t)) d\mathbf{x}(t)/dt = \mathbf{0}$ . The last equality is only satisfied if the tangent vector,  $d\mathbf{x}(t)/dt$ , is parallel to the gradient,  $\mathbf{g}(\mathbf{x}(t))$ , thus the normalized tangent at this point is,  $d\mathbf{x}(t)/dt = \mathbf{g}(\mathbf{x}(t)) \|\mathbf{g}(\mathbf{x}(t))\|^{-1}$ . Substituting this tangent vector in Eq. (10) we have that  $\mathbf{0} = \mathbf{h}_{\mathbf{e}_n}(\mathbf{x}(t)) E'(t)$ , but the vector  $\mathbf{h}_{\mathbf{e}_n}(\mathbf{x}(t)) \neq \mathbf{0}$  since at this point  $\mathbf{g}(\mathbf{x}(t)) \neq \mathbf{0}$  and  $E(t) \neq 0$  thus, to satisfy the equality it must be that  $E'(t) = 0$ . The behaviour of Eq. (10) at this point is equivalent to that explained in Mechanochemistry Section ‘A Brief Summary on the Newton Trajectory Model applied to Mechanochemistry. The existence of Bond Breaking Points’ with respect to the *optimal BBP*, since according to the previous results at this point, labeled as oBBP, the next relations are satisfied,

$$\begin{aligned} \mathbf{H}_{\mathbf{e}_n}(\mathbf{x}(t_{oBBP}), E(t_{oBBP})) \mathbf{g}(\mathbf{x}(t_{oBBP})) &= \mathbf{0}, \\ \mathbf{g}(\mathbf{x}(t_{oBBP})) &\neq \mathbf{0}. \end{aligned} \quad (18)$$

Eq. (18) is the central equation of the extended NT theory applied as model for OEEF. From these results we see that at the *optimal BBP* the growth of  $E(t)$  ends and the derivative with respect to  $t$  becomes zero. The value of  $E(t_{oBBP})$  at the *optimal BBP* can be denoted

as  $E_c$ . Substituting  $\mathbf{g}(\mathbf{x}(t_{oBBP}))$  into Eq. (7) we obtain the *optimal OEEF* with constant direction,  $\mathbf{e}^*$ . The corresponding normalized direction is denoted by  $\mathbf{e}_n^*$ . In what follows we denote by  $\mathbf{x}_{oBBP}$  the point of the curve  $\mathbf{x}(t_{oBBP})$ .

The above results can be proved in other mathematical way. To this aim, first we diagonalize the Hessian matrix,  $\mathbf{H}_{\mathbf{e}_n}(\mathbf{x}(t), E(t))$ ,

$$\mathbf{H}_{\mathbf{e}_n}(\mathbf{x}(t), E(t))\mathbf{V}(\mathbf{x}(t), E(t)) = \mathbf{V}(\mathbf{x}(t), E(t))\mathbf{H}_{\mathbf{e}_n}^D(\mathbf{x}(t), E(t)) , \quad (19)$$

where  $\mathbf{H}_{\mathbf{e}_n}^D(\mathbf{x}(t), E(t))$  is the diagonal matrix formed by the set of eigenvalues and  $\mathbf{V}(\mathbf{x}(t), E(t)) = [\mathbf{v}_1(\mathbf{x}(t), E(t)) | \cdots | \mathbf{v}_N(\mathbf{x}(t), E(t))]$  is the matrix formed by the corresponding set of orthonormal eigenvectors. Second, we change the representation of Eq. (10) to obtain a set of decoupled equations. Multiplying from the left Eq. (10) by the matrix  $\mathbf{V}^T(\mathbf{x}(t), E(t))$  and using Eq. (19) we obtain the corresponding decoupled equation

$$\mathbf{H}_{\mathbf{e}_n}^D(\mathbf{x}(t), E(t))\mathbf{c}(t) = \mathbf{b}(t)E'(t) , \quad (20)$$

where the vectors are  $\mathbf{c}(t) = \mathbf{V}^T(\mathbf{x}(t), E(t))(d\mathbf{x}(t)/dt)$  and  $\mathbf{b}(t) = \mathbf{V}^T(\mathbf{x}(t), E(t))\mathbf{h}_{\mathbf{e}_n}(\mathbf{x}(t))$ . The elements of these vectors are denoted by  $c_i(t)$  and  $b_i(t)$  respectively. Let us assume that at the point  $t$  we have that  $\text{Det}[\mathbf{H}_{\mathbf{e}_n}(\mathbf{x}(t), E(t))] = 0$ . Then this implies that an eigenvalue, say  $i$ ,  $[\mathbf{H}_{\mathbf{e}_n}^D(\mathbf{x}(t), E(t))]_{ii} = 0$ . If  $b_i(t) \neq 0$  then is the unique solution of Eq. (20)  $E'(t) = 0$ ,  $c_i(t) = 1$  and  $c_j(t) = 0$  for any  $j \neq i$ . The normalisation condition on the tangent leads to  $d\mathbf{x}(t)/dt = \mathbf{V}(\mathbf{x}(t), E(t))\mathbf{c}(t) = \mathbf{v}_i(\mathbf{x}(t), E(t))$ . Thus in this case the curve is tangent to the eigenvector with null curvature and  $E(t)$  has a turning point. In the specific case that  $\text{Det}[\mathbf{H}_{\mathbf{e}_n}(\mathbf{x}(t), E(t))] = 0$  and the eigenvector of null curvature coincides with the normalized gradient,  $\mathbf{g}(\mathbf{x}(t))/\|\mathbf{g}(\mathbf{x}(t))\|^{-1}$ , then this point corresponds to the *optimal BBP*, that is  $\mathbf{x}_{oBBP} = \mathbf{x}(t_{oBBP})$  already discussed previously. On the other hand, in the situation that  $b_i(t) = 0$ , two solutions emerge. The first one is just the solution above, and the second

one is obtained taking  $E'(t) \neq 0$  and  $c_j(t) = E'(t)b_j(t)[\mathbf{H}_{\mathbf{e}_n}^D(\mathbf{x}(t), E(t))]_{jj}^{-1}$  for any  $j \neq i$  and  $c_i(t) = 0$ . Thus we have

$$d\mathbf{x}(t)/dt = E'(t) \sum_{j \neq i} c_j(t) \mathbf{v}_j(t) = E'(t) \sum_{j \neq i} b_j(t) [\mathbf{H}_{\mathbf{e}_n}^D(\mathbf{x}(t), E(t))]_{jj}^{-1} \mathbf{v}_j(t) . \quad (21)$$

Using the normalization condition on  $d\mathbf{x}(t)/dt$  of Eq. (21) we obtain both,  $E'(t)$  and  $d\mathbf{x}(t)/dt$ . In this second case the curve bifurcates, the branch with  $E'(t) = 0$  evolves tangential to the eigenvector with null curvature while the other branch with  $E'(t) \neq 0$  evolves transversing orthogonally to this eigenvector. This case is not further discussed.

In Table 1 is summarized and compared the Newton trajectory theory for Mechanochemistry and the extended Newton trajectory theory as a model for Oriented External Electric Field problems described and discussed in the previous Sections, entitled ‘A Brief Summary on the Newton Trajectory Model applied to Mechanochemistry. The existence of Bond Breaking Points’ and ‘Optimally Oriented External Electric Field. An Extension of the Newton Trajectory Model’.

Table 1: Comparison between the Newton Trajectory model for Mechanochemistry and the Extended Newton Trajectory model for Oriented External Electric Field

Mechanochemistry	Oriented External Electric Field
Energy	
$V_{\mathbf{f}}(\mathbf{x}) = V(\mathbf{x}) - \mathbf{x}^T \mathbf{f}_n F$ where, $\mathbf{f}_n F$ , is the force	$V_{\mathbf{e}}(\mathbf{x}) = V(\mathbf{x}) - \mathbf{d}^T(\mathbf{x}) \mathbf{e}_n E$ where, $\mathbf{e}_n E$ , is the electric field
Gradient	
$\mathbf{g}_{\mathbf{f}}(\mathbf{x}) = \mathbf{g}(\mathbf{x}) - \mathbf{f}_n F$	$\mathbf{g}_{\mathbf{e}}(\mathbf{x}) = \mathbf{g}(\mathbf{x}) - [\nabla_{\mathbf{x}} \mathbf{d}^T(\mathbf{x})] \mathbf{e}_n E$
Hessian	
$\mathbf{H}_{\mathbf{f}}(\mathbf{x}) = \mathbf{H}(\mathbf{x})$ Hessian does not depend of $\mathbf{f}_n F$	$\mathbf{H}_{\mathbf{e}}(\mathbf{x}, E) = \mathbf{H}(\mathbf{x}) - \langle \mathbf{N}(\mathbf{x}) \mathbf{e}_n \rangle E$ Hessian depends of $\mathbf{e}_n E$
FDSP curve condition	
$\mathbf{g}_{\mathbf{f}}(\mathbf{x}) = \mathbf{0} \Rightarrow$ $\mathbf{g}(\mathbf{x}) = \mathbf{f}_n F$	$\mathbf{g}_{\mathbf{e}}(\mathbf{x}) = \mathbf{0} \Rightarrow$ $\mathbf{P}(\mathbf{x}) \mathbf{g}(\mathbf{x}) = \mathbf{e}_n E$
Tangent of FDSP curve	
$\mathbf{H}_{\mathbf{f}}(\mathbf{x})(d\mathbf{x}/dt) = \mathbf{f}_n F'$	$\mathbf{H}_{\mathbf{e}}(\mathbf{x}, E)(d\mathbf{x}/dt) = [\nabla_{\mathbf{x}} \mathbf{d}^T(\mathbf{x})] \mathbf{e}_n E'$
Optimal BBP condition	
$\mathbf{H}_{\mathbf{f}}(\mathbf{x}) \mathbf{g}(\mathbf{x}) = \mathbf{0} \quad \mathbf{g}(\mathbf{x}) \neq \mathbf{0}$ $\mathbf{x} = \mathbf{x}_{oBBP} \quad F_c$ maximum in the <i>optimal FDSP</i> curve	$\mathbf{H}_{\mathbf{e}}(\mathbf{x}, E) \mathbf{g}(\mathbf{x}) = \mathbf{0} \quad \mathbf{g}(\mathbf{x}) \neq \mathbf{0}$ $\mathbf{x} = \mathbf{x}_{oBBP} \quad E_c$ maximum in the <i>optimal FDSP</i> curve
Optimal external field condition	
$\mathbf{g}(\mathbf{x}_{oBBP}) = F_c \mathbf{f}_n^*$	$\mathbf{P}(\mathbf{x}_{oBBP}) \cdot \mathbf{g}(\mathbf{x}_{oBBP}) = E_c \mathbf{e}_n^*$

### 3 Two Algorithms to Find the Optimally Oriented External Electric Field.

In this Section we propose two different algorithms to first locate the  $\mathbf{x}_{oBBP}$  and, second, the corresponding *optimal OEEF*. For this purpose the set of Eqs. (7) and (18) forms a system of  $3 + N$  equations for the  $3 + N$  unknown variables, namely,  $\mathbf{x}$  and  $\mathbf{e} = (e_x, e_y, e_z)^T$ . The solution of this system of equations renders us both, the *optimal BBP*,  $\mathbf{x}_{oBBP}$ , and the *optimal OEEF*,  $\mathbf{e}^*$ . Once  $\mathbf{e}^*$  is obtained we can normalize it to  $E_c \mathbf{e}_n^*$ . The  $\mathbf{e}_n^*$  is the normalized constant direction of the *optimal OEEF* for the system under study. Before explaining the algorithms, we would like to stress that locating *optimal BBPs* in the context of different *optimal OEEFs* is more difficult than locating mechanochemical *optimal BBPs*. Indeed, in the Mechanochemistry model the gradient of the original PES is directly related with the external force with constant direction, see Eq. (2), being the reason of the simplicity of this model. However, when an OEEF with constant orientation is applied to the molecular system the relation between the gradient of the original PES and the electric field is not direct since the dipole is involved, see Eq. (6) or Eq. (7), being this the reason why in the present case is much more complicated to find the *optimal OEEF*.

The first algorithm to find the *optimal BBP* is based on the geometrical view of BBP concept. At the *optimal BBP* the Hessian,  $\mathbf{H}_{\mathbf{e}_n}(\mathbf{x}_{oBBP}, E)$  has an eigenvector with eigenvalue equal zero, which is the gradient of the original PES,  $\mathbf{g}(\mathbf{x}_{oBBP})$  (see Eq. (18)). In the subspace generated by the  $(N - 1)$  remaining eigenvectors we always find a minimum of  $V_{\mathbf{e}}(\mathbf{x})|_{\mathbf{x}=\mathbf{x}_{oBBP}}$  potential. Therefore, if we start the *optimal BBP* location from a guess point very close to it, that is to say, in the quadratic region around the *optimal BBP*, we will find it straightforwardly just by moving orthogonally to the gradient of the original PES. If, on the contrary, we start the location procedure far from the  $\mathbf{x}_{oBBP}$ , then we have to move from a FDSPs curve to another locating the BBP of each FDSP curve and making sure that

the  $V_{\mathbf{e}}(\mathbf{x})|_{\mathbf{x}=\mathbf{x}_{oBBP}}$  decreases. This iterative procedure has to be continued until the  $\mathbf{x}_{oBBP}$  is reached. See an indirect proof of this assertion and details in the Appendix.

According to that explained above, the *optimal BBP* should satisfy the conditions (18). The matrix  $\mathbf{H}_{\mathbf{e}_n}(\mathbf{x}_{oBBP}, E)$  is that given in Eq. (12) evaluated at this *optimal BBP*. We recall that at the *optimal BBP* holds that the gradient at this point,  $\mathbf{g}(\mathbf{x}_{oBBP})$ , is the eigenvector with eigenvalue equal zero of  $\mathbf{H}_{\mathbf{e}_n}(\mathbf{x}_{oBBP}, E)$  matrix. Now we propose a second algorithm to locate first the  $\mathbf{x}_{oBBP}$  and from it the *optimal OEEF*,  $\mathbf{e}^*$ . To solve this system of equations Eqs. (7) and (18) we first substitute Eq. (7) into  $\mathbf{H}_{\mathbf{e}_n}(\mathbf{x}, E)\mathbf{g}(\mathbf{x})$  where the form of  $\mathbf{H}_{\mathbf{e}_n}(\mathbf{x}, E)$  matrix is that given in Eq. (12). After some rearrangements the resulting expression is

$$\bar{\mathbf{s}}(\mathbf{x}) = [\mathbf{H}(\mathbf{x}) - \langle \mathbf{g}^T(\mathbf{x})\mathbf{N}(\mathbf{x}) \rangle \mathbf{P}(\mathbf{x})]\mathbf{g}(\mathbf{x}) . \quad (22)$$

Notice that,  $\langle \mathbf{g}^T(\mathbf{x})\mathbf{N}(\mathbf{x}) \rangle$ , is a rectangular matrix of dimension  $(N \times 3)$ . At the *optimal BBP*, the vector function  $\bar{\mathbf{s}}(\mathbf{x}_{oBBP}) = \mathbf{0}$  with  $\mathbf{g}(\mathbf{x}_{oBBP}) \neq \mathbf{0}$  (see Eq. (18)). Once the  $\mathbf{x}_{oBBP}$  is found we going back to Eq. (7) to obtain the normalized optimal constant direction for the electric field,  $\mathbf{e}_n^*$ . With  $\mathbf{x}_{oBBP}$  and  $\mathbf{e}_n^*$  vectors we can integrate Eq. (10) forward and backward to obtain the FDSP path of interest passing through  $\mathbf{x}_{oBBP}$ . To solve the problem,  $\bar{\mathbf{s}}(\mathbf{x}_{oBBP}) = \mathbf{0}$  with  $\mathbf{g}(\mathbf{x}_{oBBP}) \neq \mathbf{0}$ , some algorithms have been proposed based on Gauss–Newton methods, see e.g. ref. 58,59. These algorithms merely consist in to find the point where the function,

$$\bar{\sigma}(\mathbf{x}) = \bar{\mathbf{s}}^T(\mathbf{x})\bar{\mathbf{s}}(\mathbf{x}) , \quad (23)$$

takes the value zero since this implies that  $\bar{\mathbf{s}}(\mathbf{x}) = \mathbf{0}$  with  $\mathbf{g}(\mathbf{x}) \neq \mathbf{0}$  which occurs if  $\mathbf{x} = \mathbf{x}_{oBBP}$  is the *optimal BBP*, that it is,  $\bar{\mathbf{s}}(\mathbf{x}_{oBBP}) = \mathbf{0}$  with  $\mathbf{g}(\mathbf{x}_{oBBP}) \neq \mathbf{0}$ . We propose as an initial guess or starting point for the above mentioned Gauss–Newton methods the *optimal BBP* of an NT for the Mechanochemistry of the system under study.

Note that the above second algorithm is analogous to the one used in Mechanochemistry. There, once the mechanochemical *optimal BBP* was characterized mathematically, an algorithm to find this point was defined by looking for the zeros of the so-called  $\sigma(\mathbf{x})$ -function defined as  $\sigma(\mathbf{x}) = \mathbf{s}^T(\mathbf{x})\mathbf{s}(\mathbf{x}) = \mathbf{g}^T(\mathbf{x})\mathbf{H}^2(\mathbf{x})\mathbf{g}(\mathbf{x})$  where  $\mathbf{g}(\mathbf{x}) \neq \mathbf{0}$ .<sup>58,59</sup> At  $\mathbf{x}$  where  $\sigma(\mathbf{x}) = 0$ ,  $\mathbf{s}(\mathbf{x}) = \mathbf{H}(\mathbf{x})\mathbf{g}(\mathbf{x}) = \mathbf{0}$  and  $\mathbf{g}(\mathbf{x}) \neq \mathbf{0}$ , hence satisfying the mechanochemical *optimal BBP* condition (see Eq. (4)).

## 4 A thorough discussion of the main geometrical aspects of the oBBP and the optimal OEEF.

In this Section we will show through generic 2-dimensional examples the geometric features of the extended NT theory previously discussed as model for obtaining optimally oriented OEEFs. These examples lead to a microscopic picture of a ‘toy chemical process’ under an external electric field. We use 2-dimensional examples because they allow for an easier visualization of the force vectors, valleys and ridges of the (effective) PES. In the whole Section we use the Mathematica program in order to solve the corresponding equations.

This Section is divided in two Subsections. The first one deals with a case where the alignment between the dipole field and the reaction valley is appropriate and a solution to the optimally OEEF problem is possible. In a second example we discuss a situation where that is not possible due to a bad alignment between the dipole field and the reaction valley. This second example will be a proof that there can be situations where a gap in the FDSPs curve exists. This gap can indicate that the dipole of the molecule inhibits the application of an electric field into a desired direction. This situation emerges for many proposed putative ‘reaction pathways’ which are not steepest descent or NTs,<sup>82-84</sup> and it holds also for the often treated GEs.<sup>78,79,85,86</sup> Therefore, a conclusion of this Section will be that we must

always calculate the FDSPs associated to the optimal  $\mathbf{e}_n^*$ , viz., we have to check that the curve of FDSPs connects the minimum with the searched  $SP_1$  as well as with the global goal, i.e., the next product minimum.<sup>67,76,87</sup>

#### 4.1 The Case with Appropriate Alignment.

The PES model used for this case is taken from Fig. (2) in ref. 66. The equation of this PES is

$$V(\mathbf{x}) = V(x, y) = 4.5 (1 - \exp[-x + 1])^2 + 1.75y^2 - 0.1y^4 . \quad (24)$$

where the  $\mathbf{x} = (x, y)^T$  definition is applied in the present Section. Concerning the selected dipole field, we have selected a nonlinear dipole vector field (see Fig. (1.a)) governed by the following vectorial function:

$$\mathbf{d}(\mathbf{x}) = (d_x(x, y), d_y(x, y))^T = (\cos(0.5 (x + y)), 0.333 - 0.15 (x^2 - y))^T . \quad (25)$$

As shown in Fig. (1.b), the reaction path (RP) of this model is characterized by the straight-line, along the  $x$ -axis with  $y = 0$ . Like in a chemical example,<sup>88</sup> the dipole vector is very well aligned with the reaction path (RP). Now we show in detail the series of calculations that are necessary in the numerical development of the present extended NT theory. For this purpose we start by differentiating the dipole field with respect to the variable  $\mathbf{x}$ ,

$$\nabla_{\mathbf{x}} \mathbf{d}^T(x, y) = \begin{pmatrix} -0.5 \sin[0.5(x + y)] & -0.3x \\ -0.5 \sin[0.5(x + y)] & 0.15 \end{pmatrix} . \quad (26)$$

After that we compute the corresponding inverse matrix,

$$[\nabla_{\mathbf{x}} \mathbf{d}^T(x, y)]^{-1} = \{Det [\nabla_{\mathbf{x}} \mathbf{d}^T(x, y)]\}^{-1} \begin{pmatrix} 0.15 & 0.3x \\ 0.5 \sin [0.5 (x + y)] & -0.5 \sin [0.5 (x + y)] \end{pmatrix} \quad (27)$$

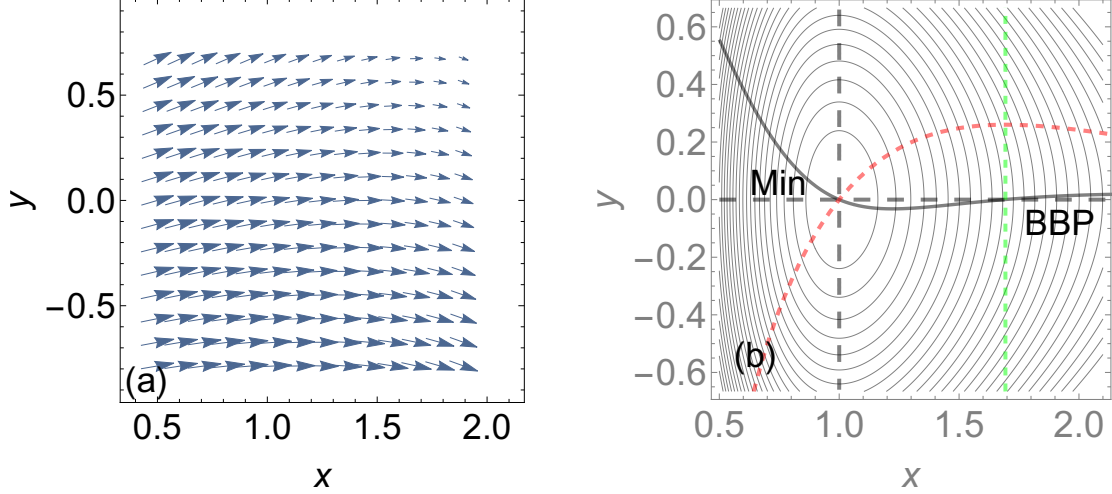


Figure 1: (a) The dipole field described by Eq. (25). (b) Three different mechanochemical NTs and one FDSP curve plotted on the original PES  $V(x, y)$  of the toy model system (Eq. (24)). The FDSP curve is computed for an OEEF associated with a given  $\mathbf{e}_n$  field with constant direction. The contours of this PES are plotted with thin black curves. The green dashed straight-line parallel to the  $y$ -axis is the manifold of points of  $V(x, y)$  where the condition  $\text{Det}[\mathbf{H}(x, y)] = 0$  is satisfied. The two bold black dashed straight-lines parallel to the  $x$ - and  $y$ -axes represent mechanochemical NTs. The continuous bold black curve is the FDSP path. Finally, the red dashed curve is a mechanochemical NT whose gradient points to the direction of  $\mathbf{e}_n$ -vector. The intersection point of the NT characterized by the  $x$ -axis at  $y = 0$  and the green line is the mechanochemical *optimal BBP* labeled by BBP. Using the gradient of  $V(x, y)$  at this BBP and Eq. (6) the  $\mathbf{e}_n$ -vector is obtained after normalization. See text for more detail.

where  $\text{Det}[\nabla_{\mathbf{x}}\mathbf{d}^T(x, y)] = -(0.075 + 0.15x)\sin[0.5(x + y)]$ . Notice that the matrix,  $[\nabla_{\mathbf{x}}\mathbf{d}^T(x, y)]^{-1}$ , corresponds to the  $\mathbf{P}(\mathbf{x})$  matrix of Eq. (8). Now, we will locate the mechanochemical *optimal BBP*, that is to say, the point satisfying Eq. (4). This point, which can be called ‘pre-optimal’ or ‘non-optimal’ BBP in the context of OEEF, will serve as an initial guess to locate the *optimal BBP* satisfying Eq. (18). The location of the mechanochemical *optimal BBP* is in this case straightforward because the RP of interest is characterized by the NT curve along the  $x$ -axis at  $y = 0$ , depicted by a black-dashed line in Fig. (1.b). As the NT curve evolves towards larger  $x$  values (satisfying Eq. (3) in all points), it intersects the manifold of points satisfying the condition  $\text{Det}[\mathbf{H}(x, y)] = 0$ , which is depicted by a green line in Fig. (1.b). The intersection point between these two curves is  $\mathbf{x}_{oBBP} = (1.693, 0.0)$  arbitrary coordinate units. This point is the mechanochemical *optimal BBP*, because the

gradient is an eigenvector with zero eigenvalue of the Hessian matrix of the original PES. The gradient vector at this point of the PES given by Eq. (24) is  $\mathbf{g}(\mathbf{x}_{oBBP}) = (2.25, 0.0)^T$  in gradient units. Thus, the  $\mathbf{g}(\mathbf{x}_{oBBP})$ -vector is the eigenvector of  $\mathbf{H}(\mathbf{x}_{oBBP})$  with eigenvalue equal zero. Using this gradient value and the inverse matrix of  $[\nabla_{\mathbf{x}} \mathbf{d}^T(x, y)]$  evaluated in the same point  $\mathbf{x}_{oBBP}$  and finally substituting these values in Eq. (7) we obtain

$$\begin{aligned} \mathbf{e} &= E \mathbf{e}_n = [\nabla_{\mathbf{x}} \mathbf{d}^T(x, y)]^{-1} \cdot \mathbf{g}(x, y) \\ &= \{Det [\nabla_{\mathbf{x}} \mathbf{d}^T(x, y)]\}^{-1} \begin{pmatrix} 0.15g_x(x, y) + 0.3xg_y(x, y) \\ 0.5 \sin[0.5(x + y)][g_x(x, y) - g_y(x, y)] \end{pmatrix}. \end{aligned} \quad (28)$$

We recall that we are interested in the OEEF model, thus we have to take the direction of the external electric field fixed. This implies that  $\mathbf{e} = E\mathbf{e}_n$ , should be a vector with constant direction, in other words  $\mathbf{e}_n$  is taken as constant vector. After normalization of the previous Eq. (28) we obtain  $\mathbf{e}_n$  which is the constant direction of the ‘non-optimal’ OEEF which is  $\mathbf{e}_n = (-0.373, -0.928)^T$ .

In two dimensional problems is possible to explicitly draw the FDSPs curve for a given electric field vector. It is defined by the set of continuous points where the gradient with respect to the coordinates of the effective potential,  $V_{\mathbf{e}}(x, y)$ , is zero. As explained in Section ‘Optimal Electric Field. An Extension of the Newton Trajectory Model’, in particular Eq. (6), this is due to the fact that in these points the gradient of the original potential,  $\nabla_{\mathbf{x}} V(x, y) = \mathbf{g}(x, y) = (g_x(x, y), g_y(x, y))^T$ , is parallel to the  $-\nabla_{\mathbf{x}} \mathbf{d}^T(x, y)\mathbf{e}_n E$ -vector and the sum of these two vectors is equal zero,

$$\begin{pmatrix} 0 \\ 0 \end{pmatrix} = \begin{pmatrix} g_x(x, y) \\ g_y(x, y) \end{pmatrix} - \begin{pmatrix} -0.5 \sin[0.5(x + y)] & -0.3x \\ -0.5 \sin[0.5(x + y)] & 0.15 \end{pmatrix} \begin{pmatrix} -0.3727 \\ -0.9279 \end{pmatrix} E. \quad (29)$$

We note that in this problem we have three unknowns,  $x, y, E$ , and two equations. Putting

$E$  to a set of ascending values starting from zero we can calculate the set of coordinates  $(x, y)$  of the FDSPs curve, as dense as we like. This procedure is equivalent to compute this path by integration of Eq. (10). The expression,

$$\begin{aligned}
\text{Traj}(x, y) &= (0.278x + 0.186 \sin[0.5(x + y)], -0.139 \\
&\quad + 0.186 \sin[0.5(x + y)])(g_y(x, y), -g_x(x, y))^T \\
&= 0.278x g_y(x, y) + 0.186 \sin[0.5(x + y)] g_y(x, y) + 0.139 g_x(x, y) \\
&\quad - 0.186 \sin[0.5(x + y)] g_x(x, y) = 0
\end{aligned} \tag{30}$$

determines the contour line zero of this ‘surface’. It is the usual manner for the calculation of NTs in a two-dimensional plane. Eq. (30) is obtained by premultiplying Eq. (29) from the left first by the invers of  $[\nabla_{\mathbf{x}} \mathbf{d}^T(x, y)]$  matrix, given in Eq. (27), and second by the transposed vector ortogonal to  $\mathbf{e}_n$ .

The representation of this curve is depicted as bold black line in Fig. (1.b). The curve, by construction, correctly crosses the green line, the line formed by the set of points where  $\text{Det}[\mathbf{H}(\mathbf{x})] = 0$ , through the point  $\mathbf{x}_{oBBP}$  because this point belongs to this green line by definition of *optimal BBP* Mechanochemistry. Having reached this point, it may be instructive to compare the latter FDSP curve, which includes the dipole–external electric field interaction term, with other NTs that, by construction, do not have this dipole term. These extra NTs are drawn in the same Fig. (1.b). Two of these curves, depicted as black dashed lines, follow the  $x$ - and  $y$ -directions, being the NT in the  $x$ -axis at  $y = 0$  direction the optimal since it passes through the mechanochemical  $\mathbf{x}_{oBBP}$ . The third NT, depicted as red dashed line, follows the  $\mathbf{e}_n$  direction, in other words at each point of this curve the gradient vector has the same direction as the  $\mathbf{e}_n$ -vector.

In the present toy model the FDSP curve shown in Fig. (1.b) has an analytical expression,

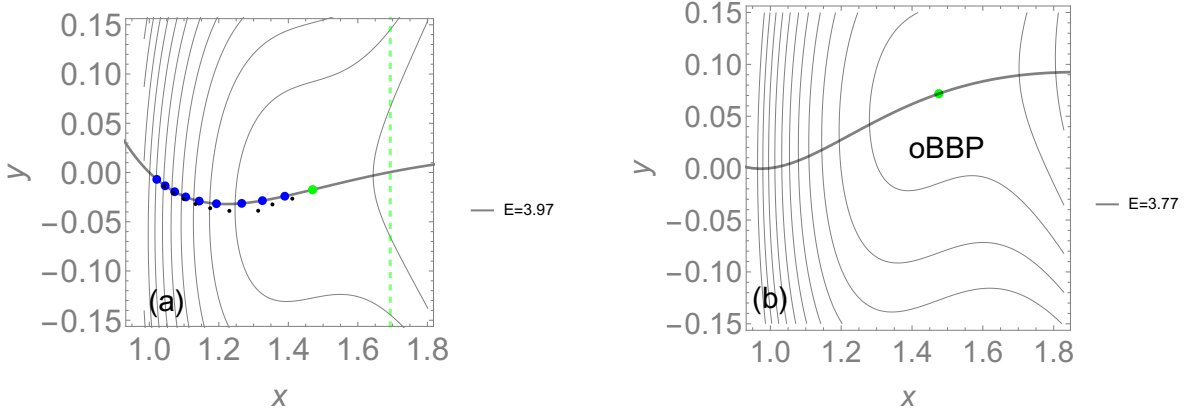


Figure 2: (a) The contour plot of the effective 2–dimensional PES,  $V_e(x, y)$ , for the OEEF with constant direction  $\mathbf{e}_n = (-0.373, -0.928)^T$  and magnitude  $E = 3.97$  arbitrary units. It displays the ‘non–optimal’ BBP (green point) located in a shoulder region. The continuous thin black curve is the analytical FDSP curve of this OEEF (evaluated using Eq. (30)). The thin black points are the predictor points obtained by Eq. (15) and the corrector points are the set of blue points computed using the algorithm described after Eq. (16). Notice that these points fall into the analytical curve. (b) Final effective PES,  $V_e(x, y)$ , corresponding to the *optimal OEEF* with constant normalized direction,  $\mathbf{e}_n^* = (-0.549, -0.836)^T$  and a modulus of  $E_c = 3.77$  arbitrary units. The *optimal BBP* of this *optimal OEEF* is reported and marked by a green point. The green dashed line represents the set of points where  $\text{Det}[\mathbf{H}(x, y)] = 0$ .

as previously seen. However, in the general case, the derivation of an analytical expression is not possible or far from trivial. Thus, a numerical method of integration may be required, as that reported in the paragraph following Eq. (16). In Fig. (2.a) we have drawn the analytical FDSPs curve plotted in thin black, together with the predictor points of the FDSP curve computed numerically using Eq. (15) in thin black color. The corresponding corrector points, which coincide with the analytical curve, are plotted in thick blue bullets. Once the FDSP curve is fully integrated the maximum  $E$  value can be identified. In the present case, the point with  $E_{max} = 3.97$  arbitrary units is located in the shoulder region (see green point in Fig. (2.a)). This means that this point is the BBP of this particular FDSP corresponding to this particular OEEF. Note that the green line in this Fig. (2.a) is the  $\text{Det}[\mathbf{H}(\mathbf{x})] = 0$ –curve of the original PES,  $V(x, y)$ . Now, we can see that the new BBP is moved with respect to the mechanochemical BBP which sits on the green line of the original PES. The constant direction field,  $\mathbf{e}_n$ , with modulus  $E_{max} = 3.97$  arbitrary units generates the effective PES,

$V_e(x, y)$ , shown in Fig. (2.a). As may be seen therein, such effective PES features a shoulder, which means that the reaction takes place without any barrier.

Although the green point of Fig. (2.a) is a BBP, it is not necessarily the optimal one. The reason is that this point has been obtained through the  $\mathbf{e}_n$ -vector associated with the mechanochemical *optimal BBP*, which may not be the optimal direction. In fact this BBP does not satisfy Eq. (18). Nevertheless, this BBP excellent guess point for finding the *optimal BBP* satisfying Eq. (18). For this purpose we have used the FindRoot procedure of the Mathematica program. The OEEF *optimal BBP* was found to have the following coordinates:  $\mathbf{x}_{oBBP} = (1.476, 0.072)^T$  arbitrary units. Again, it is observed that this BBP has slightly moved with respect to the coordinates at the ‘pre-optimal’ or ‘non-optimal’ BBP. Evaluating Eq. (7) in this point and after normalization we obtain the *optimal OEEF* direction, which in this case is  $\mathbf{e}_n^* = (-0.549, -0.836)^T$ . The norm or modulus of the field is  $E_c = 3.77$  arbitrary units. Note that this value is lower than the former. For this given dipole field and the original PES of this reaction, no lower critical amount of  $E_c$  can be found. The analytical *optimal FDSPs* curve is plotted by the thick black curve in Fig. (2.b), where the shoulder and features of the effective PES for this *optimal OEEF* are also shown. The use of the  $\bar{\sigma}(x, y)$ -function defined in the Section ‘Two Algorithms to Find the Optimally Oriented External Electric Field’ forms the basis for an alternative way to locate the *optimal BBP* of the present example. In particular, if the zeros of the  $\bar{\sigma}(x, y)$ -function are found starting from the point  $\mathbf{x}_{BBP} = (1.693, 0.0)^T$  the same *optimal BBP* ( $\mathbf{x}_{oBBP} = (1.476, 0.072)^T$ ) would be obtained. As it may be seen in Fig. (4), where the surface of the  $\bar{\sigma}(x, y)$ -function is shown, the  $\bar{\sigma}(x, y)$ -function vanishes at  $\mathbf{x}_{oBBP}$ .

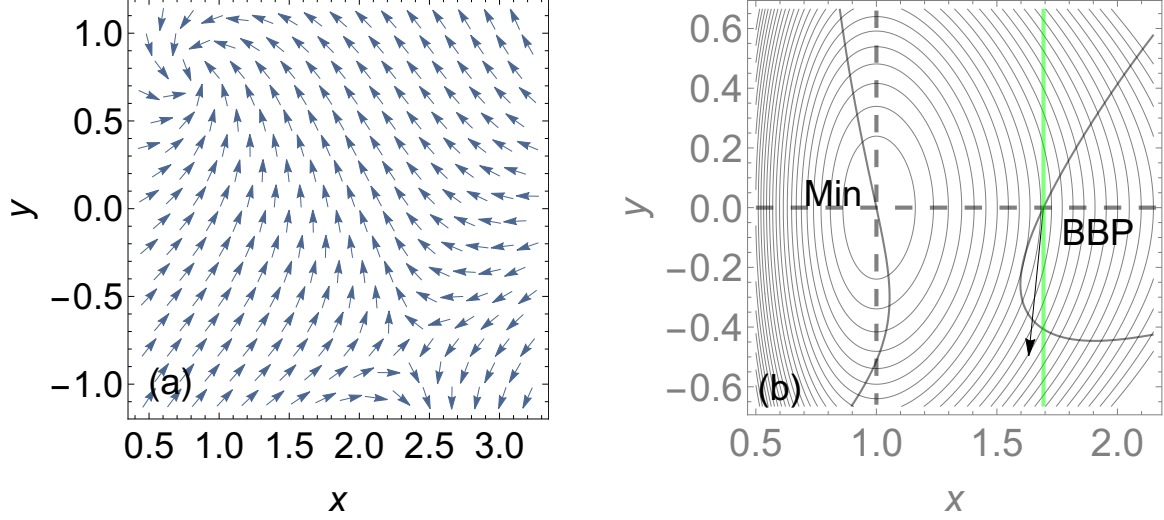


Figure 3: (a) The dipole field, Eq. (31), being quasi orthogonal to the RP, the straight-line  $x$ -axis at  $y = 0$  (bold black dashes). (b) For this dipole field, the FDSPs curve (continuous tiny bold black) associated to an  $\mathbf{e}$ -vector at the BBP shows an avoided crossing. Minimum and  $SP_1$  cannot coalesce at the BBP on this curve under this external force  $\mathbf{e}$ . The arrow is the vector  $1/2 \mathbf{e}_n$  being  $\mathbf{e}_n$  the normalized  $\mathbf{e}$ -vector and the green line represents the manifold of points where  $\text{Det}[\mathbf{H}(x, y)] = 0$ , thus this BBP is the *optimal BBP* Mechanochemistry satisfying Eq. (4).

## 4.2 Example for a missing FDSPs path between the minimum and the optimal BBP.

We present the case where there is not FDSPs curve between the minimum of the original PES to a BBP in particular to the *optimal BBP*. This proves that not always a FDSPs path exists joining the minimum with the corresponding BBP and for this reason once the BBP or the *optimal BBP* is found it is necessary to check whether the FDSPs exists or not. This point is already noted in the second paragraph of the present Section ‘A thorough discussion of the main geometrical aspects of the oBBP and the optimal OEEF’. This particular behaviour is explained through an example where the original PES is the same to that used in the Subsection ‘The Case with Appropriate Alignment’ but the dipole vector field is now that given by the expression

$$\mathbf{d}(\mathbf{x}) = \mathbf{d}(x, y) = (\cos(x + y), \sin(x - y))^T . \quad (31)$$

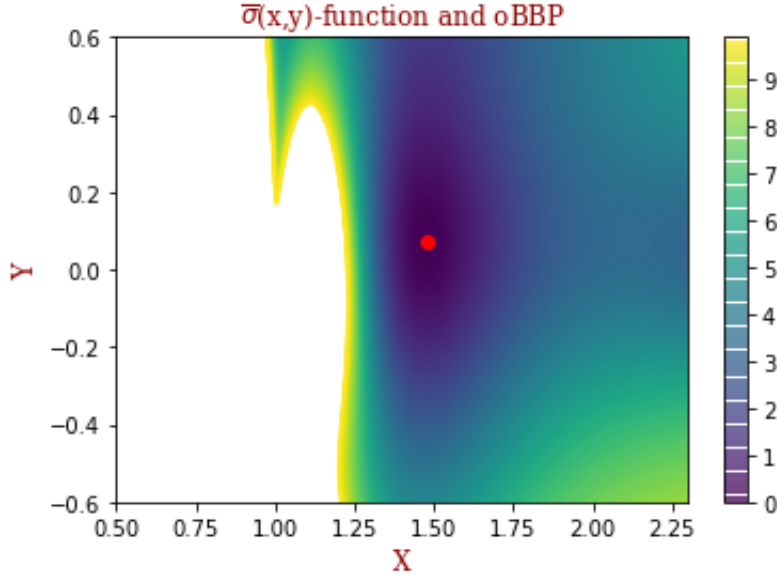


Figure 4: The  $\bar{\sigma}(x, y)$ -function for the 2-dimensional problem defined by the original PES,  $V(x, y)$ , and the dipole field,  $\mathbf{d}(x, y)$ , given by the formulas, Eqs. (24) and (25), respectively. The white part corresponds to the region of the points,  $(x, y)$ , where the  $\bar{\sigma}(x, y)$ -function takes very high values ( $\bar{\sigma}(x, y) > 10$ ). The bold red circle indicates the point where  $\bar{\sigma}(x, y) = 0$  being this point the *optimal BBP* with coordinates  $\mathbf{x}_{oBBP} = (1.476, 0.072)^T$ .

This dipole vector field is mainly orthogonal to the RP of interest, see Fig. (3.a). Notice that this RP is the straight-line  $x$ -axis at  $y = 0$ . Finding an electric field  $\mathbf{e}$  and locating the set of points satisfying Eq. (6) for this electric field we obtain a FDSPs curve that does not connect the initial minimum with the aim of the  $SP_1$  along the RP of interest, see Fig. (3.b). The electric field is found by first locating the *optimal BBP* Mechanochemistry, labeled as BBP in the figure. We recall that in this point the gradient satisfies the Eq. (4). Substituting this gradient in Eq. (7) and computing the  $\mathbf{P}(x, y)$  matrix at this point we obtain the corresponding electric field,  $\mathbf{e} = (-1.133, -9.213)^T = E \mathbf{e}_n = 9.283 (-0.122, -0.993)^T$ , in arbitrary units. Notice that in Fig. (3.b) we have used and represented the half vector  $\mathbf{e}_n$ .

One can conclude that the OEEF is not able to overcome against such a ‘false-oriented’ dipole field with respect to the RP of interest. The reason is simply the scalar product that appears in Eq. (5). If the two vectors, namely, the dipole  $\mathbf{d}(\mathbf{x})$ , and the external field  $\mathbf{e}$ , are

nearly orthogonal through the RP, then every strong force along this field  $\mathbf{e}$  may be useless. It is an unforeseen challenge of this simple method. However, at this point we emphasize that the FDSPs curve is not always the best model for a RP.

Now we try to compute the *optimal BBP* and the FDSPs curve if exists using the algorithm described in Section ‘Two Algorithms to Find the Optimally Oriented External Electric Field’ and employed in the previous Subsection ‘The Case with Appropriate Alignment’. In this case from the *optimal BBP* we obtain the electric field in arbitrary units,  $\mathbf{e}^* = (-1.447, -0.704)^T = E_c \mathbf{e}_n^* = 1.609 (-0.899, -0.438)^T$ , see Fig. (5.a). The force amount for

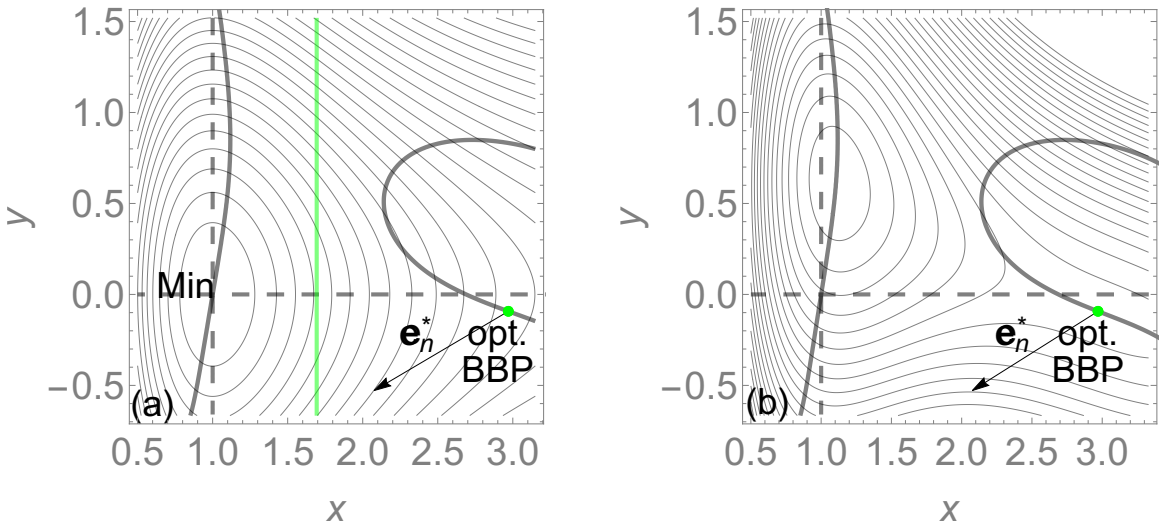


Figure 5: (a) The FDSPs curve to the normalized *optimal OEEF*,  $\mathbf{e}_n^*$ , shows an avoided crossing on the PES. (b) The FDSPs curve on the effective PES crosses the stabilized  $SP_1$  at the *optimal BBP*.

this *optimal OEEF* is very lower than that found with the *optimal BBP* Mechanochemistry along the original RP direction characterized by the straight-line  $x$ -axis at  $y = 0$ . In Fig. (5.b) we show the effective PES to force factor,  $E_c = 1.609$ , in arbitrary units and the direction of the *optimal OEEF*,  $\mathbf{e}_n^* = (-0.899, -0.438)^T$ . The new *optimal BBP*, located at the point  $\mathbf{x}_{oBBP} = (2.970, -0.093)^T$  leads to a lowering of the TS, see Fig. (5.b), however, the FDSPs curve does not joint the minimum with the TS. Thus, in this case even in the optimal situation the barrier cannot break down totally. Finally in Fig. (6) we show the

sigma function,  $\bar{\sigma}(x, y)$ , for this example and the location of the *optimal BBP*.

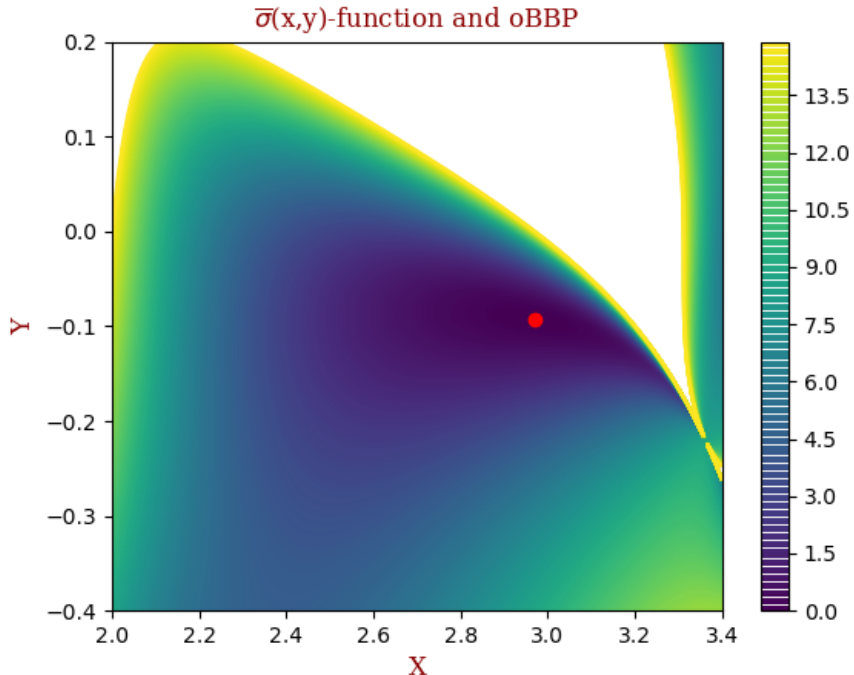


Figure 6: The  $\bar{\sigma}(x, y)$ -function for the 2-dimensional problem defined by the original PES,  $V(x, y)$ , and the dipole field,  $\mathbf{d}(x, y)$ , given by the formulas, Eqs. (24) and (31), respectively. The white part corresponds to the region of the points,  $(x, y)$ , where the  $\bar{\sigma}(x, y)$ -function takes a very high values ( $\bar{\sigma}(x, y) > 15$ ). The bold red circle indicates the point where  $\bar{\sigma}(x, y) = 0$  being this point the *optimal BBP* with coordinates  $\mathbf{x}_{oBBP} = (2.970, -0.093)^T$ .

## 5 Application of the Algorithm to Realistic Chemical Examples.

The algorithm presented will now be applied to two realistic chemical examples: i) a  $S_N2$  reaction and ii) a retrocycloaddition reaction. In both examples, the methodology used to calculate the electronic structure and the original or unperturbed  $V(\mathbf{x})$  PES *in vacuo* were performed using the B3LYP functional<sup>89</sup> and an Ahlrichs TZVP basis set,<sup>90</sup> as implemented in the Gaussian package.<sup>91</sup>

## 5.1 An $S_N2$ reaction of the amine attack on chloromethane.

We will first focus on one example of an  $S_N2$  reaction, which is one of the most fundamental and important types of chemical processes and that has already been studied in the context of electrostatic catalysis.<sup>21,38,92</sup> In particular, we will investigate the nucleophilic attack of an ammonia molecule to a chloromethane molecule (see reaction scheme in Fig. 7). In this nucleophilic methyl transfer process, the nucleophilic ammonia molecule displaces a chloride ion from the chloromethane.

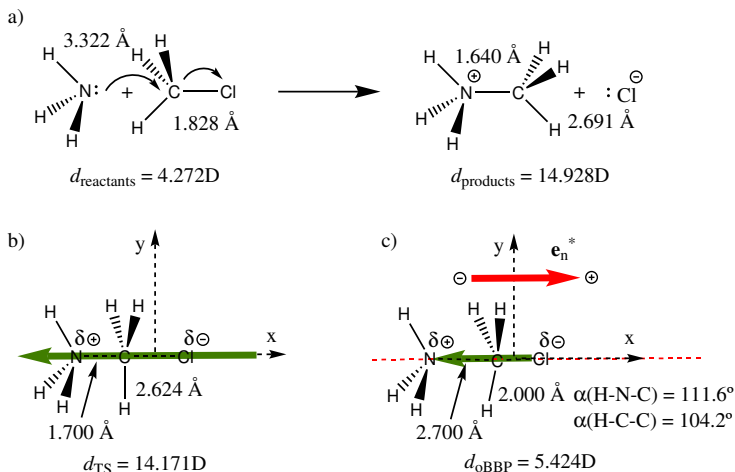


Figure 7: a) Nucleophilic-attack of amine nucleophile on chloromethane. The arrows indicate the electronic movement involved in this substitution reaction from reactants to products along with some geometrical parameters. The most relevant geometrical parameters of the transition state, TS, and the *optimal BBP* are reported in b) and c), respectively. All structures belong to the  $C_{3v}$  point group symmetry. The bond distances are given in angstroms, Å, the bond angles in degrees and the permanent dipole moment in Debyes.

Given the symmetry of the reactive molecular system (Fig. 7), it is obvious –without doing any calculation– that the EEF used to promote the reaction should be oriented along the axis passing through the  $N$ ,  $C$  and  $Cl$  atoms. Still, we will apply the theoretical model to this system to show that this is the direction of the optimal OEEF that emerges naturally without any *a priori* assumption and to show how to compute the field strength required to trigger the reaction through a barrierless or almost barrierless process. The original or unperturbed  $V(\mathbf{x})$  PES of the reaction in the subspace defined by the  $C-Cl$  and  $C-N$

distances is displayed in Fig. (8).

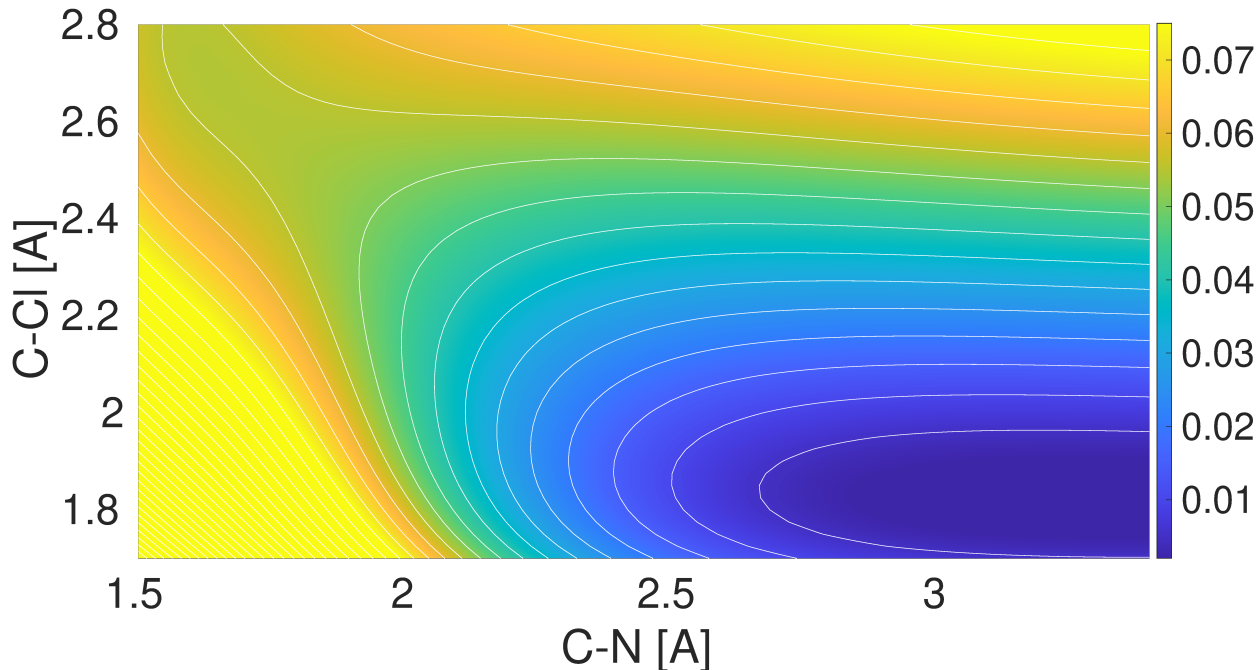


Figure 8: The original PES,  $V(\mathbf{x})$ , of the nucleophilic-attack of amine nucleophile on chloromethane. The PES is represented in the subspace characterized by the  $C-Cl$  and  $C-N$  bond distances. The TS is located at  $(1.700, 2.624)$ . The energy iso-contours are reported in atomic units.

This two-dimensional PES was computed by means of a set of constrained optimizations in which the values of the  $C-Cl$  and  $C-N$  bond distances were fixed at given values. Specifically, the two-dimensional PES was evaluated on a grid of  $45 \times 77$  points ranging from a  $C-Cl$  distance of  $1.70 \text{ \AA}$  to a  $C-Cl$  distance of  $2.80 \text{ \AA}$  and from a  $C-N$  distance of  $1.50 \text{ \AA}$  to a  $C-N$  distance of  $3.4 \text{ \AA}$ . The energies of the stationary points of the two-dimensional PES are consistent with the energies of the stationary points found upon full optimization. This, together with the fact the two-dimensional PES does not feature any discontinuity, means that the reaction can be properly described in the subspace defined by the  $C-Cl$  and  $C-N$  bond distances. Taking this into account, we will find the *optimal BBP* for the  $S_N2$  reaction in the subspace defined by these two coordinates.

As shown in the two-dimensional PES in Fig. (8), the nucleophilic attack of the ammonia molecule to chloromethane in gas phase is a highly endothermic process with a large energy barrier of 34 kcal·mol<sup>-1</sup>. Our theoretical analysis will show that an OEEF that will allow us to establish which field strength and direction should be applied to tear down the barrier. The permanent dipole moment (i.e. the dipole moment at zero field) was computed at each point of the 2-dimensional PES. The *optimal BBP* was located without considering the effects of the induced dipole moments as the present model requires. Although this might entail some degree of approximation, our objective in this Section is not to compute the *optimal OEEF* with the highest possible accuracy but to provide a proof-of-principle example of how the ansatz we have presented can be applied to a real chemical example.

The *optimal BBP* of this S<sub>N</sub>2 reaction was located through finding the zeros of the  $\bar{\sigma}(\mathbf{x}) = \bar{\mathbf{s}}^T(\mathbf{x})\bar{\mathbf{s}}(\mathbf{x})$  function, where both  $\bar{\sigma}(\mathbf{x})$  and  $\bar{\mathbf{s}}(\mathbf{x})$  were computed according to Eqs. (22) and (23), respectively (see Section ‘Two Algorithms to Find the Optimally Oriented External Electric Field’). A scheme of the configuration associated with such *optimal BBP* is displayed in Fig. (7). Once located the *optimal BBP* of the system, the *optimal OEEF* was found by solving Eq. (7). As expected, the solution of this equation yields an *optimal OEEF* that is aligned with the axis passing through the *N*, *C* and *Cl* atoms. The magnitude of the *optimal OEEF* is 0.77 V·Å<sup>-1</sup>. Note that this field strength is within the capabilities of currently available experimental setups to generate EEFs. The perturbed PES that would result from applying this field to the system is displayed in Fig. (9). This PES, which was obtained through Eq. (5), clearly shows that the *optimal OEEF* has rendered the S<sub>N</sub>2 reaction a barrierless process. A final point concerns the contribution of polarizability that has been ignored in the present approach. It can be shown that for *optimal BBP* under the present *optimal OEEF* the energetic contribution of the polarizability term is less than 20% of the permanent dipole contribution.

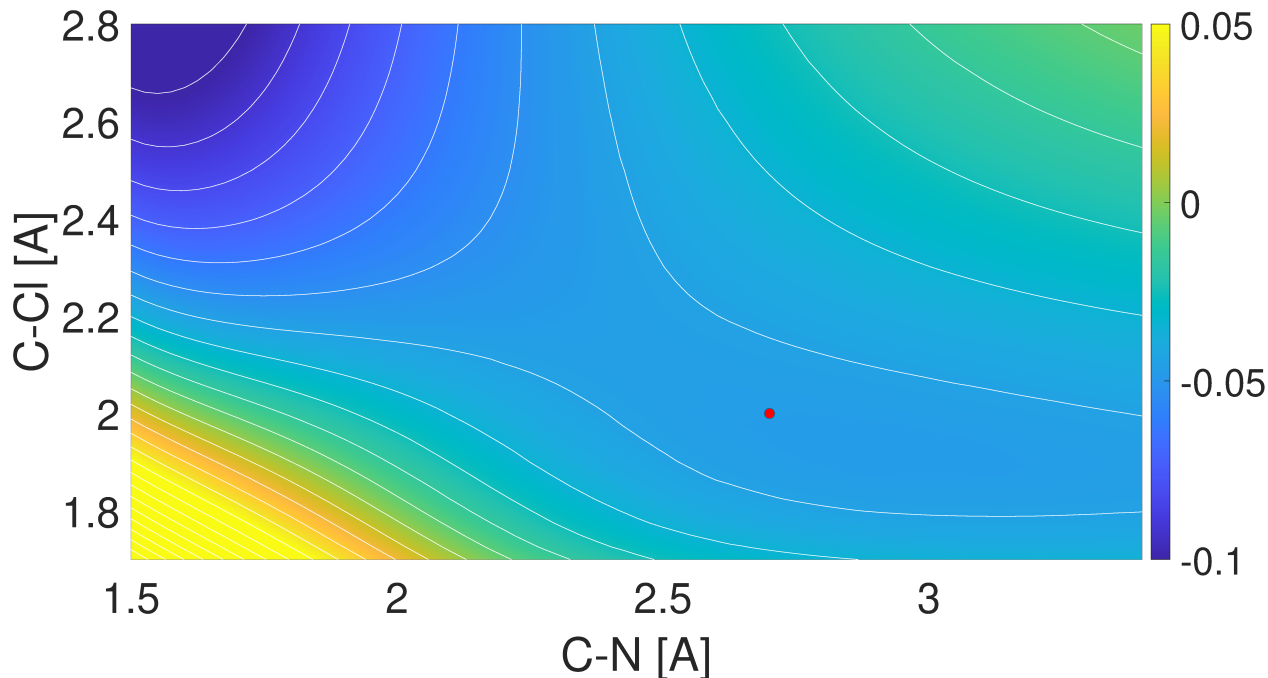


Figure 9: The perturbed PES,  $V_e(\mathbf{x})$ , resulting from applying the *optimal OEEF* to the nucleophilic-attack of amine nucleophile on chloromethane. The PES is represented in the subspace characterized by the  $C-Cl$  and  $C-N$  bond distances. The energy iso-contours are reported in atomic units. The red circle indicates the position of the *optimal BBP* located at (2.700, 2.000) and the *optimal OEEF* is aligned along the molecular axis.

## 5.2 The 1,3-Dipolar Retrocycloaddition of Isoxazole to Fulminic Acid plus Acetylene.

As a second realistic chemical example, we will focus on one reaction that belongs to the family of the 1,3-dipolar cycloadditions, which constitutes an important class of pericyclic rearrangements. In particular, we will study the Huisgen reaction, which is an example of exergonic fusion process where two unsaturated reactants come together to form five-membered heterocycles.<sup>93,94</sup> The Huisgen reaction between fulminic acid and acetylene to form isoxazole has already been studied computationally using a variety of energy functionals and basis sets.<sup>95,96</sup> The rather low energy barriers reported in previous computational studies for this reaction<sup>95,96</sup> are consistent with the experimental observation that 1,3-dipolar cycloadditions usually proceed under mild thermal conditions. Here, instead of studying the

cycloaddition reaction, we will focus our efforts in finding the *optimal OEEF* that triggers the strongly endothermic retrocycloaddition of isoxazole to fulminic acid and acetylene (see reaction scheme in Fig. (10.a)) through a barrierless process. Since the heterocycles

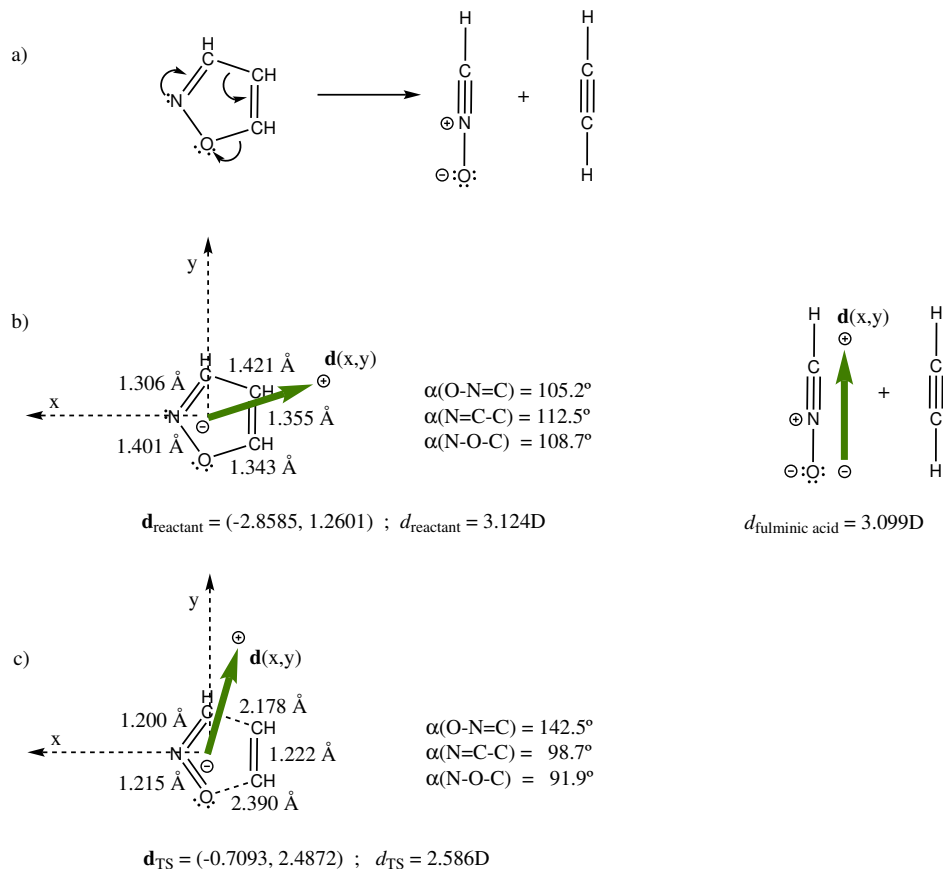


Figure 10: a) Retrocycloaddition of isoxazole to fulminic acid plus acetylene. The arrows indicate the electronic movement involved in this retrocycloaddition process leading to the products. b) The most relevant geometrical parameters of reactants and products. c) The most relevant geometrical parameters of the transition state, TS. The bond distances are given in angstroms, Å, and the bond angles in degrees. All structures belong to the  $C_s$  point group symmetry.

resulting from 1,3-dipolar reactions are commonly very stable, the energy barriers for the retrocycloaddition processes are expected to be very large,  $90 \text{ kcal}\cdot\text{mol}^{-1}$ . Accordingly, retrocycloaddition reactions do not usually occur using mild thermal activation.<sup>97,98</sup> Therefore, investigating the electrostatic catalysis of cycloreversion of heterocycles has the potential to lead to relevant novel strategies of promoting retrocycloaddition reactions. In fact, it should be mentioned that efforts have already been undertaken to explore the possibilities offered

by Mechanochemistry in the cycloreversion of triazoles.<sup>99–101</sup>

We first located the stationary points associated with the reactants and transition state configurations. As may be seen in Fig.(10.b–c), the most important geometrical changes of the molecular system during the reaction process occur in the  $C-O$  and  $C-C$  bond distances. This means that the reaction can be properly described in the subspace defined by these two coordinates. Taking this into account, we will find the *optimal BBP* for the retrocycloaddition of isoxazole in the subspace defined by these two coordinates. Working in this 2–dimensional subspace will also allow us to better illustrate the concepts and algorithms introduced in the previous Sections. The original or unperturbed  $V(\mathbf{x})$  PES in the 2–dimensional subspace was computed by means of a set of constrained optimizations in which the values of the  $C-O$  and  $C-C$  bond distances were fixed at given values. Overall, the 2–dimensional PES was evaluated on a grid of  $81 \times 81$  points ranging from a  $C-O/C-C$  distance of 1.3 Å to a  $C-O/C-C$  distance of 3.3 Å. In addition to the energy value at each point of the grid, the permanent dipole moment (i.e. the dipole moment at zero field) was also computed at each point of the 2–dimensional PES. The *optimal BBP* of the cycloreversion reaction was located through finding the zeros of the  $\bar{\sigma}(\mathbf{x}) = \bar{\mathbf{s}}^T(\mathbf{x})\bar{\mathbf{s}}(\mathbf{x})$  function, where both  $\bar{\sigma}(\mathbf{x})$  and  $\bar{\mathbf{s}}(\mathbf{x})$  were computed according to Eqs.(22) and (23), respectively (see Section ‘Two Algorithms to Find the Optimally Oriented External Electric Field’). Prior to the evaluation of the  $\bar{\sigma}(\mathbf{x})$ –function, the components of the dipole moment at each point of the 2–dimensional PES in the subspace spanned by the  $C-O$  and  $C-C$  bond distances were obtained by projecting the dipole moment given in Cartesian coordinates to the vectors associated with the two bond distances. The red bold circle shown on the unperturbed PES of Fig.(11) marks a configuration for which the  $\bar{\sigma}(\mathbf{x})$ –function is zero. To check whether or not this configuration corresponds to the *optimal OEEF* connecting the reactants and TS configurations, the *optimal FDSP* curve was evaluated. To this end, we first calculated – by means of Eq.(7) – the electric field vector,  $\mathbf{e}^* = \mathbf{e}_n^*E$ , that converts the red

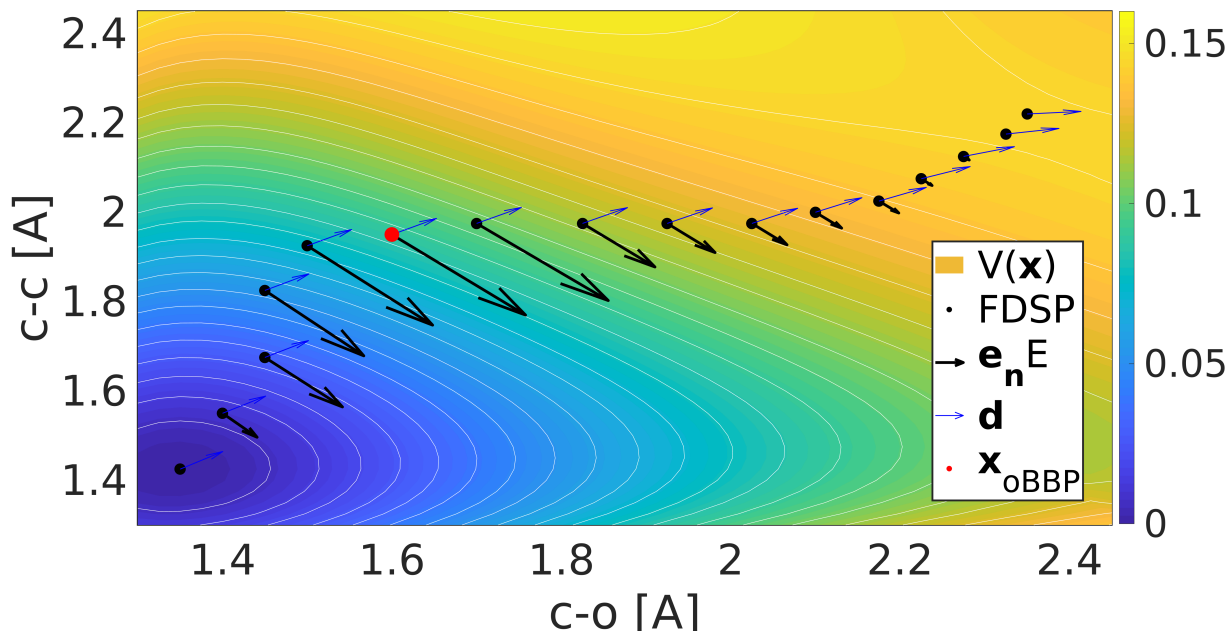


Figure 11: The *optimal FSDP* path on the original  $V(\mathbf{x})$  PES joining the point associated to the isoxazole, located at (1.343, 1.421), with the region associated to the fulminic acid plus acetylene in the top right of panel. The last point is near to the TS structure, located at (2.390, 2.178), and is part of the shoulder until the products region. The *optimal FSDP* is projected on a 2-dimensional subspace characterized by the coordinates,  $C-O$  and  $C-C$  bond lengths, of the original PES,  $V(\mathbf{x})$ . The *optimal OEEF*,  $\mathbf{e}^* = E\mathbf{e}_n^*$ , is also depicted with black arrows at some different points of the optimal FSDP curve. Notice the constant direction of electric field vector,  $\mathbf{e}^*$ , and the change of field magnitude  $E$  along the *optimal FSDP* curve. The normalized *optimal OEEF*-vector,  $\mathbf{e}_n^*$ , is that obtained from the normalized electric field computed at the *optimal BBP*, marked by a red bold circle, being the coordinates of this point, (1.600, 1.925). The glide vector of  $\mathbf{e}_n^*$  is (0.0540,  $-0.9985$ ) with respect to the external Cartesian axes, compare Fig. (12). Notice that the *optimal BBP* is a point of this curve much closer to the reactant structure than the TS. The energy iso-contours are also reported in atomic units, indicating that the optimal FSDP travels through a valley region.

bold circle into a stationary point on the perturbed PES. Let us remember that, in the original PES,  $\nabla_{\mathbf{x}}V(\mathbf{x}_{oBBP}) \neq \mathbf{0}$ , but after the effect of the electric field in the perturbed PES,  $\nabla_{\mathbf{x}}V_e(\mathbf{x}_{oBBP}) = \mathbf{0}$ . This  $\mathbf{e}^*$ -vector is shown with a black arrow starting from the red point, *optimal BBP*, in Fig. (11). Subsequently, the *optimal FSDP* curve was obtained by solving Eq. (6) for a very dense set of different magnitudes of  $E$ , from zero up to maximum value along the normalized *optimal OEEF*-vector,  $\mathbf{e}_n^*$ . For each different magnitude, Eq. (6) yielded two solutions: one solution corresponds to a configuration lying closer to

the TS configuration (i.e, a configuration resulting from the reaction going forward) while the other solution corresponds to a configuration lying closer to the reactants configuration (i.e, a configuration resulting from the reaction going backwards). Note that solving Eq. (6) for different values of  $E$  amounts to numerically integrating Eq. (10) or Eq. (14). The set of black circles of Fig. (11) are points of the *optimal FDSP* curve obtained from different values of  $E$ . The fact that the *optimal FDSP* curve connects the reactants and TS configurations passing through the red bold circle proves that this point is the *optimal BBP* of the reaction. A scheme of the configuration associated with such *optimal BBP* is displayed in Fig. (12).

Having demonstrated that the red point in Fig. (11) is the *optimal BBP* of the system, it can be concluded that the black arrow starting at this point is the vector associated with the *optimal OEEF* ( $\mathbf{e}^* = \mathbf{e}_n^* E$ ). If we take this vector and evaluate the perturbed PES according to Eq. (5), we obtain the perturbed PES displayed in Fig. (13). As clearly seen in this figure, the *optimal BBP* sits on top of a plateau and the barrier between reactants and TS has vanished. The application of the *optimal OEEF* has thus rendered the cycloreversion reaction a barrierless process. The direction of such *optimal OEEF* with respect to the molecular orientation is displayed in Fig. (12). The field strength required to remove the barrier is  $19 \text{ V}\cdot\text{\AA}^{-1}$ . Clearly, this is an extremely large value from a chemical point of view, much larger than the fields generated in commonly employed experimental setups (which can reach values of the order of  $1.0 \text{ V}\cdot\text{\AA}^{-1}$ ). The reason for the large field strength is twofold: i) the very high energy barrier for the cycloreversion process ( $90 \text{ kcal}\cdot\text{mol}^{-1}$  in vacuum) at zero field; ii) the relatively small (much smaller, for instance, than in the  $S_N2$  reaction previously studied) variation of the dipole as the system evolves from reactants to the TS passing through the *optimal BBP*. It is also clear that other effects (e.g. induced dipole) not considered in our model would become important if such large fields were applied to the system. In fact, these large fields could even trigger other processes, such as the ionization of the isoxazole molecule. That said, we will not examine the role of these

effects/processes because the main objective of this subsection is not to study in detail the electrostatic catalysis of the cycloreversion of isoxazole but to illustrate how our new theoretical model can be employed to a real chemical example where establishing the direction of the *optimal OEEF* without any calculation is not obvious. In any case, this direction will provide the optimal reduction of the barrier for any applied EEF. It should be stressed that the *optimal OEEF* found for the retro-cycloaddition reaction does not need to be equal to the *optimal OEEF* required to eliminate the barrier for the cycloaddition reaction. In order to find the *optimal OEEF* for the cycloaddition reaction, we should first locate the optimal BBP for this process, which would be located somewhere in between the TS and the products (fulminic acid and acetylene) configuration. In general, the *optimal OEEF* for a given chemical process will be different from the *optimal OEEF* for the corresponding backward process.

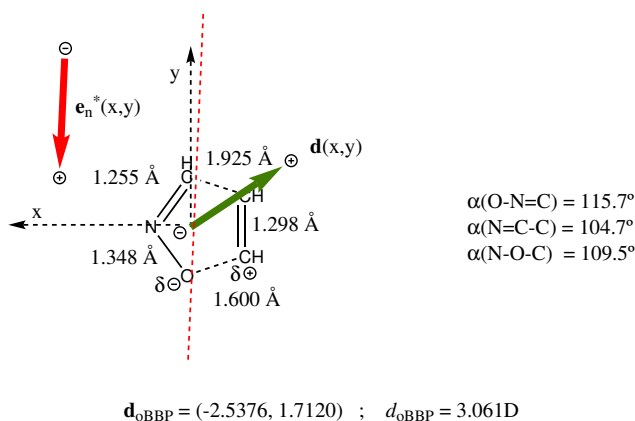


Figure 12: *Optimal BBP* of the transformation from isoxazole to fulminic acid plus acetylene. The dipole moment orientation,  $\mathbf{d}(x, y)$ , (green color) and the optimal direction of the OEEF,  $\pm\mathbf{e}^*$ , (red color) are reported. The orientation of these two vectors corresponds to the original Cartesian coordinates and they form  $56.0^\circ$  and  $3.1^\circ$  with the  $y$ -axis, respectively (i.e.  $52.9^\circ$  between them). The dipole is given in debyes (D) whereas the coordinates in angstroms, ( $\text{\AA}$ ). From the normalized electric field, we obtain the normalized direction *optimal OEEF*,  $\mathbf{e}_n^* = (0.0540, -0.9985)$  with respect to the external Cartesian axes. Notice that the electronic movement displayed in Fig. (10.a) is favoured by a field applied in this direction.

To conclude this Section, we will describe the OEEF protocol for the retrocycloaddition reaction as the ‘simplest quantum problem’, that is, the evolution of a two-states system

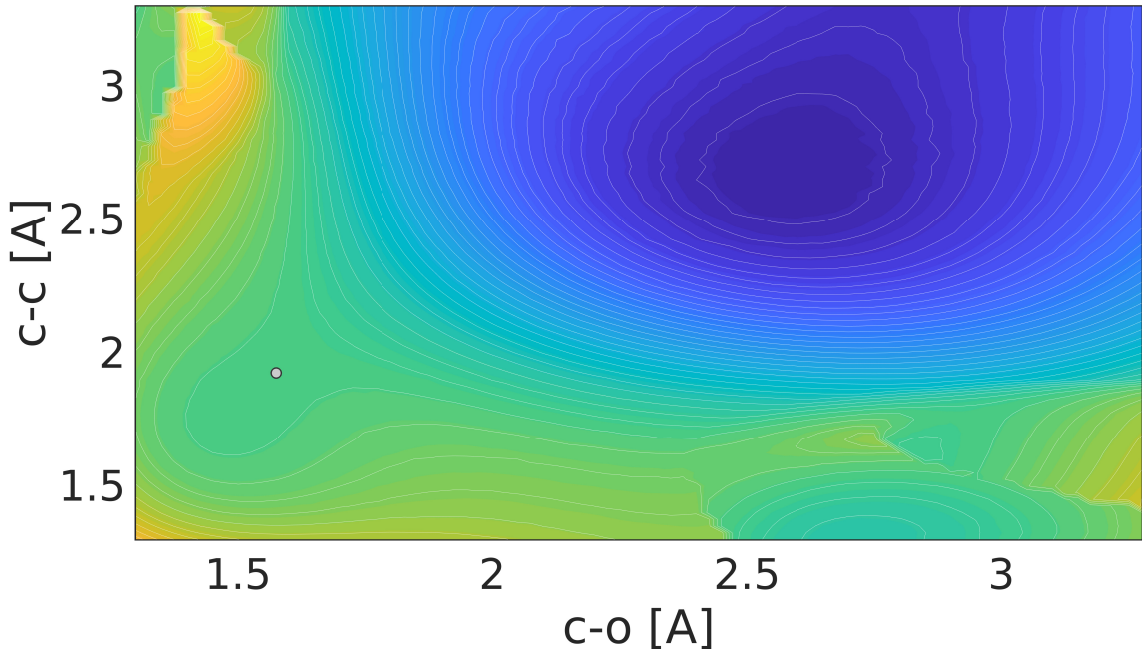


Figure 13: Perturbed PES resulting from applying the *optimal OEEF* to the cycloreversion reaction, showing that the barrier is removed. The grey bold circle indicates the position of the *optimal BBP*.

through the reaction coordinate  $s$ , as illustrated in Fig. (14), where the energies are expressed in arbitrary units and the normalized reaction coordinate. Here the two states  $|\varphi_{CT}(s)\rangle$  and  $|\varphi_{HL}(s)\rangle$ , the diabatic levels, are coupled via the electronic Born–Oppenheimer Hamiltonian characterized by the instantaneous adiabatic levels of the molecular system  $|\psi_0(s)\rangle$  and  $|\psi_1(s)\rangle$  corresponding to the ground and excited electronic states, respectively. Fig. (14) shows the spectrum energy profile of the system with an avoided crossing of the adiabatic levels  $|\psi_0(s)\rangle$  and  $|\psi_1(s)\rangle$  at some intermediate  $s$  between 0 and 1. The OEEF can be seen as a protocol that drives the molecular system through an anticrossing region in such a way that at the end of the reaction ( $s = 1$ ) the final state product  $|\Psi_P(1)\rangle$  is as close as possible to the adiabatic ground state  $|\psi_0(1)\rangle$  (fulminic acid plus acetylene), aiming that  $|\langle\Psi_P(1)|\psi_0(1)\rangle|^2 = 1$ . Assuming that the molecular system is initially described as the adiabatic ground state  $|\Psi_R(0)\rangle = |\psi_0(0)\rangle$ , there are infinitely many paths in the space and electronic configuration connecting  $|\psi_0(0)\rangle$  with  $|\psi_0(1)\rangle$ . In Fig. (14) we show two classes

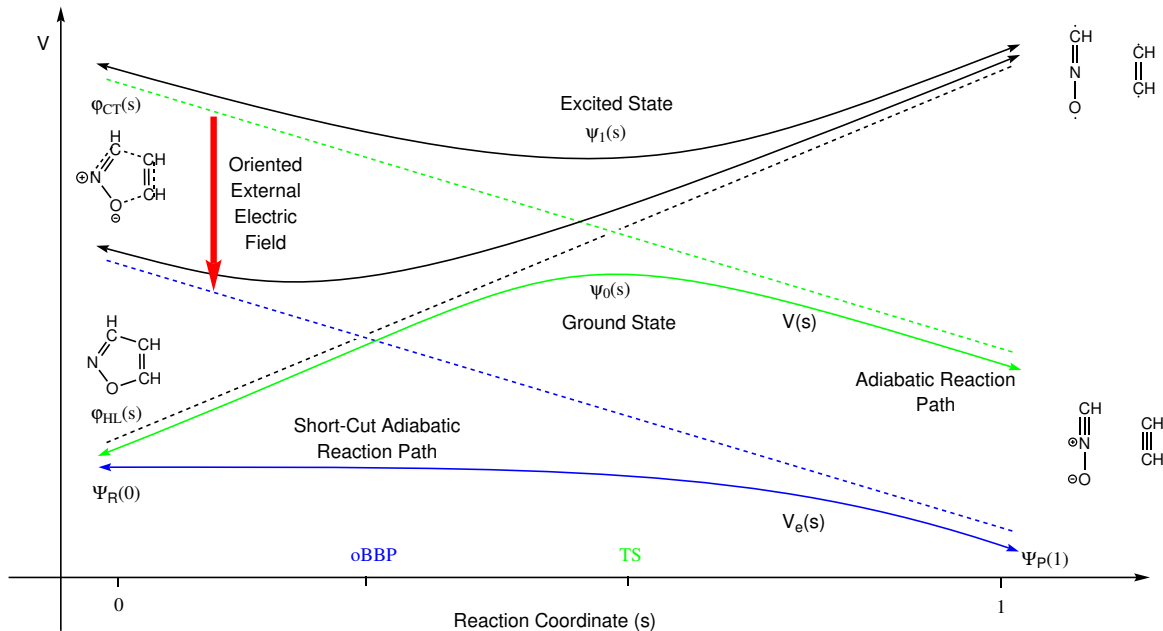


Figure 14: The bare (diabatic) electronic states  $|\varphi_{CT}(s)\rangle$  and  $|\varphi_{HL}(s)\rangle$  (dashed lines) are coupled to give the adiabatic electronic states  $|\psi_0(s)\rangle$  and  $|\psi_1(s)\rangle$  (continuous curves). The adiabatic electronic states have an energy gap where the diabatic levels cross, in a point of  $s$  between 0 and 1. The green and blue continuous curves indicate the transformations discussed in the main text: the adiabatic protocol where the system follows the non-perturbed ground electronic state (green continuous curve),  $V(s)$ , and the ‘short-cut adiabatic path’ (blue continuous curve) where the system follows the perturbed ground electronic state due to an OEEF,  $V_e(s)$ .

of such transformations. The first, allowing the possibility to follow the adiabatic ground state  $|\psi_0(s)\rangle$  for all  $s$  represented by the energy profile of a RP on the original  $V(\mathbf{x})$  (green continuous curve) and second, the effect of an OEEF minimizing the adiabatic state barrier, we call this ‘short-cut adiabatic reaction path’. This ‘short-cut adiabatic reaction path’ represented by a blue continuous curve is the energy profile of the *optimal FDSP* on the effective potential,  $V_e(\mathbf{x})$ , of Fig.(11). Notice that while the ‘short-cut adiabatic’ concept introduced in Quantum Mechanics is related with quantum dynamical propagation,<sup>102</sup> in the present model it consists in a non-dynamical evolution along a path on a stationary electronic state PES satisfying the Born–Oppenheimer approximation.<sup>103</sup> This picture provides an interesting connection in order to interpret electronic processes in chemical reactivity.

## 6 Conclusions.

In this article, we have presented a novel theoretical model aimed at providing new tools to establish which is the optimal direction in which an external electric field should be applied to accelerate a given reaction in the most efficient form. The model we have introduced is a generalization of the NT model used in Mechanochemistry. The central concept of our model is the so-called *optimal BBP*. If we consider a reaction that starts from one particular reactants configuration and passes through a particular TS configuration, the *optimal BBP* for this reaction is a point on the PES lying somewhere in between the reactant and the TS configuration with unique topological properties. At the *optimal BBP*, the gradient of the original PES is an eigenvector with a null eigenvalue of the perturbed Hessian of the system (i.e., the Hessian that takes into account the original or non-perturbed PES of the system and the action of the electric field on the electric dipole of the system).

The *optimal BBP* of a reaction can be located by means of an algorithm that explores iteratively different FDSP curves (and hence different directions of the OEEF) or by an algorithm that minimizes a specific positively defined function that goes to zero at the coordinates of *optimal BBPs*. The location of the *optimal BBP* of a given reaction is very important because this point on the PES contains all the information required to obtain the *optimal OEEF* for the reaction. Indeed, the gradient of the original PES at the *optimal BBP* combined with the pseudoinverse matrix of the derivatives of the dipole of the system with respect to its coordinates at this point provide the direction in which an OEEF should be applied to render a given chemical reaction a barrierless process with the minimal intensity of the field.

The FDSP curves constitute another essential element of our theoretical model. Once the *optimal BBP* has been determined, it is mandatory to evaluate the FDSP curve using the direction of the *optimal OEEF* associated with the *optimal BBP*. If this curve leads

continuously from the reactant configuration to the TS and product configurations passing through the *optimal BBP*, then the *optimal OEEF* is able to promote a reaction by rendering it barrierless. If, on the contrary, the FDSP curve has a gap, an avoided crossing or the TS configuration does not show a stabilization, or the curve of the FDSPs deviates after the TS uphill to a second-order saddle point, then the electric field will not be able to efficiently promote the reaction. This will happen, for instance, when the direction of the dipole field and the direction of the RP of the reaction of interest are more or less orthogonal.

The conceptual framework commonly used to rationalize or to predict the effect of an OEEF on the activation energy of a given reaction considers exclusively two configurations of the PES, namely, the reactants and TS configurations. The results presented in this article make a strong case for considering also another configuration of the PES – the *optimal BBP* – specially when it comes to predicting the most efficient way to induce electrostatic catalysis. Within the commonly-used framework, it is accepted that the electrostatic catalysis of a reaction can be achieved by means of two mechanisms: either an electric-field-induced stabilization of the TS with respect to the reactants configuration, or by an electric-field-induced destabilization of the reactants with respect to the TS.<sup>88</sup> Considering *optimal BBPs* is so important for an optimal control of OEEFs in the sense of minimizing the effective potential because this amounts to simultaneously exploiting the two mechanisms by which electrostatic catalysis occurs.

An OEEF with sufficient intensity and a properly chosen direction will distort the structure of the reactants so that this configuration will move uphill on the PES towards the TS configuration. As the intensity of the field increases, the reactant configuration will move closer to the TS configuration. Likewise, the OEEF with the properly chosen direction will move the TS configuration downhill the PES towards the reactants configuration. As the intensity of the field increases, the TS configuration will move closer to the reactants config-

uration. For a sufficiently high intensity, the reactants and TS configurations will coalesce. If the two configurations meet at the *optimal BBP*, it means that the OEEF acting on the system is the optimal one for the given reaction. This image of both the reactants and TS configurations moving closer to each other and eventually coalescing at the *optimal BBP* as a result of the *optimal OEEF* allows one to better understand why the model based on the *optimal BBP* provides the theoretical foundations for a conceptual framework in which the two mechanisms of electrostatic catalysis naturally come together to ensure the maximum efficiency of an OEEF. Therefore, we think that the burgeoning field of electrostatic catalysis by means of OEEFs would benefit by embracing the concept of *optimal BBP*. In view of the increasingly-recognized key role played by the electrostatic fields exerted by the active sites of enzymes in their catalytic activity, the concept of *optimal BBP* might well be relevant in the field of enzymatic catalysis.

With reference to the interaction of the OEEF and the molecular system, the theoretical model we have presented takes into consideration the permanent dipole moment of the system. As such, the model in its current version does not take into account the effect of the induced dipole moment, which stems from the polarizability tensor. Accordingly, the accuracy of the results provided by the model (in terms of the direction and strength of the *optimal BBP*) will be better when the effects of the induced dipole become less important (i.e. with small to moderate field strengths and small to moderate polarizabilities). In future works, we will endeavor to include the effects of induced dipoles in the theoretical model. We will also endeavor to generalize the model in order to establish the direction of the *optimal OEEF* in those cases in which the electric field cannot completely eliminate the energy barrier but just lower it.

## 7 Appendix.

Let be  $\mathbf{x}_{BBP}$  any BBP on a FDSPs path with  $\mathbf{H}_{\mathbf{e}_n}(\mathbf{x}_{BBP}, E) \mathbf{g}(\mathbf{x}_{BBP}) \neq \mathbf{0}$  and any corresponding normalized search direction  $\mathbf{e}_n$ . Now, the gradient,  $\mathbf{g}(\mathbf{x}_{BBP})$ , does not point into the direction of the tangent of the corresponding FDSPs curve, since  $\mathbf{H}_{\mathbf{e}_n}(\mathbf{x}_{BBP}, E) (d\mathbf{x}/dt) = \mathbf{0}$ . We move to a new point in the coordinate space, downhill or uphill to the gradient direction of the original PES, with a small step  $\tilde{\mathbf{x}}_{\pm} = \mathbf{x}_{BBP} \pm \epsilon \mathbf{g}(\mathbf{x}_{BBP})$ . The new points will be on other FDSPs curves corresponding to new directions  $\tilde{\mathbf{e}}_{n\pm}$  and different  $\mathbf{x}_{BBP\pm}$  points. Once we have move from the previous FDSPs curve to new ones, we can search for the corresponding new BBPs, ( $\hat{\mathbf{x}}_{\pm}$ ) fulfilling both  $\nabla_{\mathbf{x}} V_{\tilde{\mathbf{e}}_{\pm}}(\hat{\mathbf{x}}_{\pm}) = \mathbf{0}$ , and  $Det[\mathbf{H}_{\tilde{\mathbf{e}}_n}(\hat{\mathbf{x}}_{\pm}, E)] = 0$ . Taking into account that we have moved from one FDSPs curve to new ones, in the general case it follows that,

$$V_{\mathbf{e}}(\mathbf{x}_{BBP}) \neq V_{\tilde{\mathbf{e}}_{\pm}}(\hat{\mathbf{x}}_{\pm}) . \quad (32)$$

If the minus solution is lower in energy than the plus solution, ( $V_{\tilde{\mathbf{e}}_-}(\hat{\mathbf{x}}_-) < V_{\tilde{\mathbf{e}}_+}(\hat{\mathbf{x}}_+)$ ), or viceversa, it follows that the first BBP was not the *optimal BBP* of the problem because this corresponds to a lower value of  $V_{\mathbf{e}}(\mathbf{x})$ . If the gradient of the original PES at the new located BBP point is parallel to the tangent of the FDSPs, by virtue of Eq. (18), then this is the *optimal BBP* which leads to the *optimal OEEF*. In other words, back-search for the BBP gives the same BBP, being the optimal one. Otherwise, we have to continue the iterative procedure moving to other points following the gradient of the original PES as explained above.

## Acknowledgement

The authors thank the financial support from the Spanish Ministerio de Economía y Competitividad, Projects No. PID2019-109518GB-I00, PID2020-117803GB-I00, CTQ2017-87773-P/AEI/ FEDER, Spanish Structures of Excellence María de Maeztu program through grant

## References

- (1) Shaik, S., Stuyver, T., Eds. *Effects of Electric Fields on Structure and Reactivity*; Theoretical and Computational Chemistry Series; The Royal Society of Chemistry, 2021; pp 001–428.
- (2) Shaik, S.; Mandal, D.; Ramanan, R. Oriented electric fields as future smart reagents in chemistry. *Nat. Chem.* **2016**, *8*, 1091–1098.
- (3) Shaik, S.; Ramanan, R.; Danovich, D.; Mandal, D. Structure and reactivity/selectivity control by oriented–external electric fields. *Chem. Soc. Rev.* **2018**, *47*, 5125–5145.
- (4) Shaik, S.; Danovich, D.; Joy, J.; Wang, Z.; Stuyver, T. Electric–Field Mediated Chemistry: Uncovering and Exploiting the Potential of (Oriented) Electric Fields to Exert Chemical Catalysis and Reaction Control. *J. Am. Chem. Soc.* **2020**, *142*, 12551–12562.
- (5) Stuyver, T.; Danovich, D.; Joy, J.; Shaik, S. External electric field effects on chemical structure and reactivity. *WIREs Comput. Mol. Sci.* **2020**, *10*, e1438.
- (6) Stark, J. Observation of the Separation of Spectral Lines by an Electric Field. *Nature* **1913**, *92*, 401–401.
- (7) Fried, S. D.; Boxer, S. G. Measuring Electric Fields and Noncovalent Interactions Using the Vibrational Stark Effect. *Acc. Chem. Res.* **2015**, *48*, 998–1006.
- (8) Drexler, C. I.; Cracchiolo, O. M.; Myers, R. L.; Okur, H. I.; Serrano, A. L.; Corcelli, S. A.; Cremer, P. S. Local Electric Fields in Aqueous Electrolytes. *J. Phys. Chem. B* **2021**, *125*, 8484–8493.

- (9) Yang, D.; Wu, S. *Fundamentals of Liquid Crystal Devices*; John Wiley & Sons, Ltd, 2014; Chapter 4, pp 127–148.
- (10) Son, Y.; Cohen, M. L.; Louie, S. G. Half-metallic graphene nanoribbons. *Nature* **2006**, *444*, 347–349.
- (11) Velpula, G.; Teyssandier, J.; De Feyter, S.; Mali, K. S. Nanoscale Control over the Mixing Behavior of Surface–Confined Bicomponent Supramolecular Networks Using an Oriented External Electric Field. *ACS Nano* **2017**, *11*, 10903–10913.
- (12) Simpson, G. J.; García-López, V.; Daniel Boese, A.; Tour, J. M.; Grill, L. How to control single–molecule rotation. *Nat. Commun.* **2019**, *10*, 4631.
- (13) Alemani, M.; Peters, M. V.; Hecht, S.; Rieder, K.; Moresco, F.; Grill, L. Electric Field–Induced Isomerization of Azobenzene by STM. *J. Am. Chem. Soc.* **2006**, *128*, 14446–14447.
- (14) Mangel, S.; Skripnik, M.; Polyudov, K.; Dette, C.; Wollandt, T.; Punke, P.; Li, D.; Urcuyo, R.; Pauly, F.; Jung, S. J.; Kern, K. Electric-field control of single–molecule tautomerization. *Phys. Chem. Chem. Phys.* **2020**, *22*, 6370–6375.
- (15) Bi, H.; Palma, C.; Gong, Y.; Hasch, P.; Elbing, M.; Mayor, M.; Reichert, J.; Barth, J. V. Voltage–Driven Conformational Switching with Distinct Raman Signature in a Single–Molecule Junction. *J. Am. Chem. Soc.* **2018**, *140*, 4835–4840.
- (16) Jaroš, A.; Bonab, E. F.; Straka, M.; Foroutan–Nejad, C. Fullerene–Based Switching Molecular Diodes Controlled by Oriented External Electric Fields. *J. Am. Chem. Soc.* **2019**, *141*, 19644–19654.
- (17) Zang, Y.; Zou, T.; Fu, Ng, F.; Fowler, B.; Yang, J.; Li, H.; Steigerwald, M. L.; Nuckolls, C.; Venkataraman, L. Directing isomerization reactions of cumulenes with electric fields. *Nat. Commun.* **2019**, *10*, 4482.

- (18) Harzmann, G. D.; Frisenda, R.; van der Zant, H. S. J.; Mayor, M. Single-Molecule Spin Switch Based on Voltage-Triggered Distortion of the Coordination Sphere. *Angew. Chem. Int. Ed.* **2015**, *54*, 13425–13430.
- (19) Ciampi, S.; Darwish, N.; Aitken, H. M.; Díez-Pérez, I.; Coote, M. L. Harnessing electrostatic catalysis in single molecule, electrochemical and chemical systems: a rapidly growing experimental tool box. *Chem. Soc. Rev.* **2018**, *47*, 5146–5164.
- (20) Zhang, S.; Chen, W.; Shi, H.; Zhou, W.; Zhang, J. Theoretical Studies of the Influence of an Intermolecular Force and an Electric Field on the Methanol Raman Spectrum. *J. Phys. Chem. C* **2020**, *124*, 6955–6963.
- (21) Andrés, J.; Lledós, A.; Duran, M.; Bertrán, J. Electric fields acting as catalysts in chemical reactions. An ab initio study of the walden inversion reaction. *Chem. Phys. Lett.* **1988**, *153*, 82–86.
- (22) Carbonell, E.; Duran, M.; Lledos, A.; Bertran, J. Catalysis of Friedel–Crafts reactions by electric fields. *J. Phys. Chem.* **1991**, *95*, 179–183.
- (23) Shaik, S.; de Visser, S. P.; Kumar, D. External Electric Field will Control the Selectivity of Enzymatic-Like Bond Activations. *J. Am. Chem. Soc.* **2004**, *126*, 11746–11749.
- (24) Hirao, H.; Chen, H.; Carvajal, M. A.; Wang, Y.; Shaik, S. Effect of External Electric Fields on the C–H Bond Activation Reactivity of Nonheme Iron-oxo Reagents. *J. Am. Chem. Soc.* **2008**, *130*, 3319–3327.
- (25) Meir, R.; Chen, H.; Lai, W.; Shaik, S. Oriented Electric Fields Accelerate Diels–Alder Reactions and Control the endo/exo Selectivity. *ChemPhysChem* **2010**, *11*, 301–310.
- (26) Lai, W.; Chen, H.; Cho, K.; Shaik, S. External Electric Field Can Control the Catalytic Cycle of Cytochrome P450cam: A QM/MM Study. *J. Phys. Chem. Lett.* **2010**, *1*, 2082–2087.

- (27) Aragonés, A. C.; Haworth, N. L.; Darwish, N.; Ciampi, S.; Bloomfield, N. J.; Wallace, G. G.; Diez-Perez, I.; Coote, M. L. Electrostatic catalysis of a Diels–Alder reaction. *Nature* **2016**, *531*, 88–91.
- (28) Zhang, L.; Laborda, E.; Darwish, N.; Noble, B. B.; Tyrell, J. H.; Pluczyk, S.; Le Brun, A. P.; Wallace, G. G.; Gonzalez, J.; Coote, M. L.; Ciampi, S. Electrochemical and Electrostatic Cleavage of Alkoxyamines. *J. Am. Chem. Soc.* **2018**, *140*, 766–774.
- (29) Huang, X.; Tang, C.; Li, J.; Chen, L.-C.; Zheng, J.; Zhang, P.; Le, J.; Li, R.; Li, X.; Liu, J.; Yang, Y.; Shi, J.; Chen, Z.; Bai, M.; Zhang, H.-L.; Xia, H.; Cheng, J.; Tian, Z.; Hong, W. Electric field-induced selective catalysis of single-molecule reaction. *Sci. Adv.* **2019**, *5*.
- (30) Akamatsu, M.; Sakai, N.; Matile, S. Electric-Field-Assisted Anion- $\pi$  Catalysis. *J. Am. Chem. Soc.* **2017**, *139*, 6558–6561.
- (31) Vogel, Y. B.; Zhang, L.; Darwish, N.; Gonçalves, V. R.; Le Brun, A.; Gooding, J. J.; Molina, A.; Wallace, G. G.; Coote, M. L.; Gonzalez, J.; Ciampi, S. Reproducible flaws unveil electrostatic aspects of semiconductor electrochemistry. *Nat. Comm.* **2017**, *8*, 2066.
- (32) Gorin, C. F.; Beh, E. S.; Bui, Q. M.; Dick, G. R.; Kanan, M. W. Interfacial Electric Field Effects on a Carbene Reaction Catalyzed by Rh Porphyrins. *J. Am. Chem. Soc.* **2013**, *135*, 11257–11265.
- (33) Klinska, M.; Smith, L. M.; Gryn'ova, G.; Banwell, M. G.; Coote, M. L. Experimental demonstration of pH-dependent electrostatic catalysis of radical reactions. *Chem. Sci.* **2015**, *6*, 5623–5627.
- (34) Blyth, M. T.; Coote, M. L. A pH-Switchable Electrostatic Catalyst for the Diels–Alder

- Reaction: Progress toward Synthetically Viable Electrostatic Catalysis. *J. Org. Chem.* **2019**, *84*, 1517–1522.
- (35) Yu, S.; Vermeeren, P.; Hamlin, T. A.; Bickelhaupt, F. M. How Oriented External Electric Fields Modulate Reactivity. *Chem. Eur. J.* **2021**, *27*, 5683–5693.
- (36) Aitken, H. M.; Coote, M. L. Can electrostatic catalysis of Diels–Alder reactions be harnessed with pH–switchable charged functional groups? *Phys. Chem. Chem. Phys.* **2018**, *20*, 10671–10676.
- (37) Bhattacharyya, K.; Karmakar, S.; Datta, A. External electric field control: driving the reactivity of metal–free azide–alkyne click reactions. *Phys. Chem. Chem. Phys.* **2017**, *19*, 22482–22486.
- (38) Ramanan, R.; Danovich, D.; Mandal, D.; Shaik, S. Catalysis of Methyl Transfer Reactions by Oriented External Electric Fields: Are Gold–Thiolate Linkers Innocent? *J. Am. Chem. Soc.* **2018**, *140*, 4354–4362.
- (39) Mattioli, E. J.; Bottoni, A.; Zerbetto, F.; Calvaresi, M. Oriented External Electric Fields Affect Rate and Stereoselectivity of Electrocyclic Reactions. *J. Phys. Chem. C* **2019**, *123*, 26370–26378.
- (40) Stuyver, T.; Danovich, D.; De Proft, F.; Shaik, S. Electrophilic Aromatic Substitution Reactions: Mechanistic Landscape, Electrostatic and Electric–Field Control of Reaction Rates, and Mechanistic Crossovers. *J. Am. Chem. Soc.* **2019**, *141*, 9719–9730.
- (41) Joy, J.; Stuyver, T.; Shaik, S. Oriented External Electric Fields and Ionic Additives Elicit Catalysis and Mechanistic Crossover in Oxidative Addition Reactions. *J. Am. Chem. Soc.* **2020**, *142*, 3836–3850.
- (42) Acosta–Silva, C.; Bertran, J.; Branchadell, V.; Oliva, A. Kemp Elimination Reaction Catalyzed by Electric Fields. *ChemPhysChem* **2020**, *21*, 295–306.

- (43) Kempfer–Robertson, E. M.; Thompson, L. M. Effect of Oriented External Electric Fields on the Photo and Thermal Isomerization of Azobenzene. *J. Phys. Chem. A* **2020**, *124*, 3520–3529.
- (44) Chen, Y.; Liu, Y.; Zhang, Q.; Yan, Y.; Yin, W. Degradation of bromobenzene via external electric field. *J. Theor. Comput. Chem.* **2020**, *19*, 2050004.
- (45) Che, F.; Gray, J. T.; Ha, S.; McEwen, J. Improving Ni Catalysts Using Electric Fields: A DFT and Experimental Study of the Methane Steam Reforming Reaction. *ACS Catal.* **2017**, *7*, 551–562.
- (46) Che, F.; Gray, J. T.; Ha, S.; Kruse, N.; Scott, S. L.; McEwen, J. Elucidating the Roles of Electric Fields in Catalysis: A Perspective. *ACS Catal.* **2018**, *8*, 5153–5174.
- (47) Wang, Z.; Danovich, D.; Ramanan, R.; Shaik, S. Oriented–External Electric Fields Create Absolute Enantioselectivity in Diels–Alder Reactions: Importance of the Molecular Dipole Moment. *J. Am. Chem. Soc.* **2018**, *140*, 13350–13359.
- (48) Jutglar Lozano, K.; Santiago, R.; Ribas–Arino, J.; Bromley, S. T. Twistable dipolar aryl rings as electric field actuated conformational molecular switches. *Phys. Chem. Chem. Phys.* **2021**, *23*, 3844–3855.
- (49) Warshel, A. Energetics of enzyme catalysis. *Proc. Natl. Acad. Sci. U.S.A* **1978**, *75*, 5250–5254.
- (50) Warshel, A.; Sharma, P. K.; Kato, M.; Xiang, Y.; Liu, H.; Olsson, M. H. M. Electrostatic basis for enzyme catalysis. *Chem. Rev.* **2006**, *106*, 3210–3235.
- (51) Fried, S. D.; Bagchi, S.; Boxer, S. G. Extreme electric fields power catalysis in the active site of ketosteroid isomerase. *Science* **2014**, *346*, 1510–1514.
- (52) Fried, S. D.; Boxer, S. G. Electric Fields and Enzyme Catalysis. *Ann. Rev. Biochem.* **2017**, *86*, 387–415.

- (53) Bhowmick, A.; Sharma, S. C.; Head–Gordon, T. The Importance of the Scaffold for de Novo Enzymes: A Case Study with Kemp Eliminase. *J. Am. Chem. Soc.* **2017**, *139*, 5793–5800.
- (54) Welborn, V. V.; Head–Gordon, T. Fluctuations of Electric Fields in the Active Site of the Enzyme Ketosteroid Isomerase. *J. Am. Chem. Soc.* **2019**, *141*, 12487–12492.
- (55) Welborn, V. V.; Ruiz Pestana, L.; Head–Gordon, T. Computational optimization of electric fields for better catalysis design. *Nat. Catal.* **2018**, *1*, 649–655.
- (56) Dittner, M.; Hartke, B. Globally Optimal Catalytic Fields–Inverse Design of Abstract Embeddings for Maximum Reaction Rate Acceleration. *J. Chem. Theory Comput.* **2018**, *14*, 3547–3564.
- (57) Dittner, M.; Hartke, B. Globally optimal catalytic fields for a Diels–Alder reaction. *J. Chem. Phys.* **2020**, *152*, 114106–114121.
- (58) Bofill, J. M.; Ribas–Ariño, J.; García, S. P.; Quapp, W. An Algorithm to Locate Optimal Bond Breaking Points on a Potential Energy Surface. *J. Chem. Phys.* **2017**, *147*, 152710–152719.
- (59) Bofill, J. M.; Valero, R.; Ribas–Ariño, J.; Quapp, W. Barnes Update Applied in the Gauss–Newton Method: An Improved Algorithm to Locate Bond Breaking Points. *J. Chem. Theory Comput.* **2021**, *17*, 996–1007.
- (60) Beyer, M. K. The mechanical strength of a covalent bond calculated by density functional theory. *J. Chem. Phys.* **2000**, *112*, 7307–7312.
- (61) Quapp, W.; Hirsch, M.; Imig, O.; Heidrich, D. Searching for Saddle Points of Potential Energy Surfaces by Following a Reduced Gradient. *J. Comput. Chem.* **1998**, *19*, 1087–1100.

- (62) Quapp, W.; Hirsch, M.; Heidrich, D. Bifurcation of Reaction Pathways: the Set of Valley Ridge Inflection Points of a Simple Three-dimensional Potential Energy Surface. *Theor. Chem. Acc.* **1998**, *100*, 285–299.
- (63) Bofill, J. M.; Anglada, J. M. Finding Transition States using Reduced Potential-energy Surfaces. *Theor. Chem. Acc.* **2001**, *105*, 463–472.
- (64) Crehuet, R.; Bofill, J. M.; Anglada, J. M. A new Look at the Reduced-gradient-following Path. *Theor. Chem. Acc.* **2002**, *107*, 130–139.
- (65) Quapp, W. Reduced Gradient Methods an their Relation to Reaction Paths. *J. Theoret. Comput. Chem.* **2003**, *2*, 385–418.
- (66) Quapp, W.; Bofill, J. M. A contribution to a theory of mechanochemical pathways by means of Newton trajectories. *Theor. Chem. Acc.* **2016**, *135*, 113–129.
- (67) Quapp, W.; Bofill, J. M.; Ribas–Ariño, J. Analysis of the Acting Forces in a Theory of Catalysis and Mechanochemistry. *J. Phys. Chem. A* **2017**, *121*, 2820–2838.
- (68) Ribas–Ariño, J.; Shiga, M.; Marx, D. Understanding Covalent Mechanochemistry. *Angew. Chem., Int. Ed.* **2009**, *48*, 4190.
- (69) Ong, M. T.; Leiding, J.; Tao, H.; Virshup, A. M.; Martínez, T. J. First Principles Dynamics and Minimum Energy Pathways for Mechanochemical Ring Opening of Cyclobutene. *J. Am. Chem. Soc.* **2009**, *131*, 6377–6379.
- (70) Pauling, L. Molecular architecture and biological reactions. *Chem. Eng. News* **1946**, *24*, 1375–1377.
- (71) Hirsch, M.; Quapp, W. Reaction Channels of the Potential Energy Surface: Application of Newton Trajectories. *J. Molec. Struct., THEOCHEM* **2004**, *683*, 1–13.

- (72) Konda, S. S. M.; Avdoshenko, S. M.; Makarov, D. E. Exploring the Topography of the Stress-modified Energy Landscapes of Mechanosensitive Molecules. *J. Chem. Phys.* **2014**, *140*, 104114.
- (73) Heidrich, D.; Kliesch, W.; Quapp, W. *Properties of Chemically Interesting Potential Energy Surfaces*; Springer: Berlin, Heidelberg, 1991.
- (74) Thom, R. *Structural Stability and Morphogenesis: An Outline of a General Theory of Models*; Addison-Wesley: Reading, MA, 1989.
- (75) Gilmore, R. *Catastrophe Theory for Scientists and Engineers*; Dover, New York, 1993.
- (76) Quapp, W.; Bofill, J. M. Reaction Rates in a Theory of Mechanochemical Pathways. *J. Comput. Chem.* **2016**, *37*, 2467–2478.
- (77) Sun, J.-Q.; Ruedenberg, K. Gradient Extremals and Steepest Descent Lines on Potential Energy Surfaces. *J. Chem. Phys.* **1993**, *98*, 9707–9714.
- (78) Quapp, W. Gradient Extremals and Valley Floor Bifurcation on Potential Energy Surfaces. *Theoret. Chim. Acta* **1989**, *75*, 447–460.
- (79) Bofill, J. M.; Quapp, W.; Caballero, M. The Variational Structure of Gradient Extremals. *J. Chem. Theory Comput.* **2012**, *8*, 927–935.
- (80) Penrose, R. A Generalized Inverse for Matrices. *Math. Proc. Cambridge Philos. Soc.* **1955**, *51*, 406–413.
- (81) Ben-Israel, A.; Greville, T. *Generalized Inverses: Theory and Applications*; John Wiley, 1974.
- (82) Bofill, J. M.; Quapp, W. Calculus of Variations as a basic Tool for Modeling of Reaction Paths and Localization of Stationary Points on Potential Energy Surfaces. *Molec. Phys.* **2020**, *118*, e1667035.

- (83) Quapp, W.; Bofill, J. M. Comment on "Exploring Potential Energy Surface with External Forces". *J. Computat. Theor. Chem.* **2020**, *16*, 811–815.
- (84) Quapp, W.; Bofill, J. M. Some Mathematical Reasoning on the Artificial Force Induced Reaction Method. *J. Comput. Chem.* **2020**, *41*, 629–634.
- (85) Quapp, W.; Imig, O.; Heidrich, D. In *The Reaction Path in Chemistry: Current Approches and Perspectives*; Heidrich, D., Ed.; Kluwer Academic Publishers, Dordrecht, 1995; pp 137–160.
- (86) Hirsch, M.; Quapp, W. The reaction pathway of a Potential Energy surface as curve with induced tangent. *Chem. Phys. Lett.* **2004**, *395*, 150–156.
- (87) Quapp, W.; Bofill, J. M.; Ribas-Ariño, J. Towards a Theory of Mechanochemistry—Simple Models from the Early Beginnings. *Int. J. Quant. Chem.* **2018**, *118*, e25775.
- (88) Stuyver, T.; Ramanan, R.; Mallick, D.; Shaik, S. Oriented (Local) Electric Fields Drive the Millionfold Enhancement of the H-Abstraction Catalysis Observed for Synthetic Metalloenzyme Analogues. *Angew. Chem. Int. Ed.* **2020**, *59*, 7915–7920.
- (89) Becke, A. D. Density-functional thermochemistry. III. The role of exact exchange. *J. Chem. Phys.* **1993**, *98*, 5648–5652.
- (90) Schäfer, A.; Huber, C.; Ahlrichs, R. Fully optimized contracted Gaussian basis sets of triple zeta valence quality for atoms Li to Kr. *J. Chem. Phys.* **1994**, *100*, 5829–5835.
- (91) Frisch, M. J.; Trucks, G. W.; Schlegel, H. B.; Scuseria, G. E.; Robb, M. A.; Cheeseman, J. R.; Scalmani, G.; Barone, V.; Mennucci, B.; Petersson, G. A.; Nakatsuji, H.; Caricato, M.; Li, X.; Hratchian, H. P.; Izmaylov, A. F.; Bloino, J.; Zheng, G.; Sonnenberg, J. L.; Hada, M.; Ehara, M.; Toyota, K.; Fukuda, R.; Hasegawa, J.; Ishida, M.; Nakajima, T.; Honda, Y.; Kitao, O.; Nakai, H.; Vreven, T.; Montgomery, J. A., Jr.;

- Peralta, J. E.; Ogliaro, F.; Bearpark, M.; Heyd, J. J.; Brothers, E.; Kudin, K. N.; Staroverov, V. N.; Kobayashi, R.; Normand, J.; Raghavachari, K.; Rendell, A.; Burant, J. C.; Iyengar, S. S.; Tomasi, J.; Cossi, M.; Rega, N.; Millam, J. M.; Klene, M.; Knox, J. E.; Cross, J. B.; Bakken, V.; Adamo, C.; Jaramillo, J.; Gomperts, R.; Stratmann, R. E.; Yazyev, O.; Austin, A. J.; Cammi, R.; Pomelli, C.; Ochterski, J. W.; Martin, R. L.; Morokuma, K.; Zakrzewski, V. G.; Voth, G. A.; Salvador, P.; Dannenberg, J. J.; Dapprich, S.; Daniels, A. D.; Farkas, ; Foresman, J. B.; Ortiz, J. V.; Cioslowski, J.; Fox, D. J. Gaussian 09 Revision E.01. Gaussian Inc. Wallingford CT 2009.
- (92) Wang, C.; Danovich, D.; Chen, H.; Shaik, S. Oriented External Electric Fields: Tweezers and Catalysts for Reactivity in Halogen–Bond Complexes. *J. Am. Chem. Soc.* **2019**, *141*, 7122–7136.
- (93) Huisgen, R. 1,3–Dipolar Cycloadditions. Past and Future. *Angew. Chem. Int. Ed.* **1963**, *2*, 565–598.
- (94) Rostovtsev, V. V.; Green, L. G.; Fokin, V. V.; Sharpless, K. B. A Stepwise Huisgen Cycloaddition Process: Copper(I)–Catalyzed Regioselective “Ligation” of Azides and Terminal Alkynes. *Angew. Chem. Int. Ed.* **2002**, *41*, 2596–2599.
- (95) McDouall, J. J. W.; Robb, M. A.; Niazi, U.; Bernardi, F.; Schlegel, H. B. An MC–SCF Study of the Mechanisms for 1,3–Dipolar Cycloadditions. *J. Am. Chem. Soc.* **1987**, *109*, 4642–4648.
- (96) Nguyen, M. T.; Chandra, A. K.; Sakai, S.; Morokuma, K. Another Look at the Mechanism of the Concerted 1,3–Dipolar Cycloaddition of Fulminic Acid to Acetylene. *J. Org. Chem.* **1999**, *64*, 65–69.
- (97) Kolb, H. C.; Finn, M. G.; Sharpless, K. B. Click Chemistry: Diverse Chemical Function from a Few Good Reactions. *Angew. Chem. Int. Edit.* **2001**, *40*, 2004–2021.

- (98) Kempe, K.; Krieg, A.; Becer, C. R.; Schubert, U. S. Clicking on/with polymers: a rapidly expanding field for the straightforward preparation of novel macromolecular architectures. *Chem. Soc. Rev.* **2012**, *41*, 176–191.
- (99) Schütze, D.; Holz, K.; Müller, J.; Beyer, M. K.; Lüning, U.; Hartke, B. Pinpointing Mechanochemical Bond Rupture by Embedding the Mechanophore into a Macrocycle. *Angew. Chem. Int. Edit.* **2015**, *54*, 2556–2559.
- (100) Krupika, M.; Dopieralski, P.; Marx, D. Unclicking the Click: Metal-Assisted Mechanochemical Cycloreversion of Triazoles Is Possible. *Angew. Chem. Int. Edit.* **2017**, *56*, 7745–7749.
- (101) Stauch, T.; Dreuw, A. Force-induced retro-click reaction of triazoles competes with adjacent single-bond rupture. *Chem. Sci.* **2017**, *8*, 5567–5575.
- (102) Guéry-Odelin, D.; Ruschhaupt, A.; Kiely, A.; Torrontegui, E.; Martínez-Garaot, S.; Muga, J. G. Shortcuts to adiabaticity: Concepts, methods, and applications. *Rev. Mod. Phys.* **2019**, *91*, 045001–045054.
- (103) Messiah, A. *Quantum Mechanics*; Dover books; Dover Publications, 1999.

## Graphical TOC Entry

